On the Properties of Discrete Spatial Filters for CFD

A. Báez Vidal[a], O. Lehmkuhl[b], F.X. Trias[a], C.D. Pérez-Segarra[a,*]

[a] *Heat and Mass Transfer Technological Center, Polytechnical University of Catalonia, TR4 Building, 11th Colon Str. 08222 Terrassa (Barcelona), Spain*
[b] *TermoFluids S. L. 97-E Jacquard Av. 08222 Terrassa (Barcelona), Spain*

Abstract

The spatial filtering of variables in the context of Computational Fluid Dynamics (CFD) is a common practice. Most of the discrete filters used in CFD simulations are locally accurate models of continuous operators. However, when filters are adaptative, i.e. the filter width is not constant, or meshes are irregular, discrete filters sometimes break relevant global properties of the continuous models they are based on. For example, the principle of maxima and minima reduction or conservation are eventually infringed. In this paper, we analyze the properties of analytic continuous convolution filters and extract those we consider to define filtering. Then, we impose the accomplishment of these properties on explicit discrete filters by means of constraints. Three filters satisfying the derived conditions are deduced and compared to common differential discrete CFD filters on synthetic fields. Tests on the developed discrete filters show the fulfillment of the imposed properties. In particular, the problem of maxima and minima generation is resolved for physically relevant cases. The tests are conducted on the basis of the eigenvectors of graph Laplacian matrices of meshes. Thus, deep insight into the relations between filtering and oscillation growth on general meshes is provided. Further tests on singularity fields and on isentropic vortices have also been conducted to evaluate the performance of filters on basic CFD fields. Results confirm that imposing the proposed conditions makes discrete filters properties consistent with those of the continuous ones.

Keywords: Filters, CFD, LES, Finite Volumes

1. Introduction

The Navier-Stokes Equations (NSE) form a system of Partial Differential Equations that describes the conservation of momentum, mass and energy of a Newtonian fluid using the Eulerian formulation. Even though they were formulated over 150 years ago, NSE are still a formidable mathematical problem for which analytical solutions have been found for some simple cases only. For the vast majority of scientific or engineering problems involving fluids, empirical

*Corresponding author
Email addresses: aleix@cttc.upc.edu (A. Báez Vidal), oriol@termofluids.com (O. Lehmkuhl), xavi@cttc.upc.edu (F.X. Trias), cttc@cttc.upc.edu (C.D. Pérez-Segarra)
URL: http://www.termofluids.com (O. Lehmkuhl), http://www.cttc.upc.edu (C.D. Pérez-Segarra)

data or simulations results are required.

CFD is the branch of Fluid Dynamics that produces and studies the algorithms needed to numerically simulate problems involving fluid flow. Due to Kolmogorov's power law of the turbulent flow spectrum, the full resolution of most of the fluid flow problems requires unaffordable computational resources and computation times. Modeling the smallest turbulent flow scales can reduce the required computational resource and make problems affordable. Nevertheless, as the computer resource required for CFD is still large, algorithms must be efficient to allow the most accurate simulations of the most complex problems in the shortest possible time for a given computer capacity.

Among the common operations of CFD, we focus on filtering fields on non-uniform discrete spatial domains. In this paper we gather the essential properties of this operation in the continuous field and propose constraints to transfer them to filters in discrete spaces. Spatial filtering is also common in other fields of science and technology. However doing it on non-uniform spatial domains (unstructured meshes) is very particular of CFD, so alien literature does not directly apply.

The use of spatial filtering operations on CFD has several objectives. The most important and known use of filters in CFD is filtering the NSE to obtain the Large Eddy Simulations (LES) equations [20]. This is a rather theoretical use for which filters should be low-pass, linear, normalized and commutative with differentiation. Convolution filters match these properties. In practice, LES is not often performed with explicit filtering as it is assumed that discrete differential operators have a filtering effect [20] and eliminating explicit filtering reduces computation effort. Since the computation cost of convolution filters would make explicitly filtered LES unaffordable for most of the flows of interest and implicitly filtered LES has been reported [14] to be inconsistent with the filtered NSE, alternatives to convolution filters have been investigated. One of the main difficulties when designing appropriate filters for explicit LES is that if the simulated turbulent flow is inhomogeneous and thus is the mesh, the error due to commutation between discrete filtering and differential operators can become harmful. Ghosal and Moin [8] elaborated a theory to estimate such error on non-uniform meshes and later Vasilyev et al. [28] proposed a method based on the cancellation of the filter kernel moments to derive filters that can reduce commutation error to any order desired. Based on the same theory, methods to construct filters with similar characteristics on unstructured meshes were more recently proposed [15, 10]. Even though this family of filters is shown to fulfill the commutation error reduction goal, the transfer fictions are greater than 1 [28] for some wave scales when their stencils are not symmetric and their transfer function is not positive if the order of the commutation error is greater than 2. Henceforth, reducing commutation error to less than second order results on the not fulfillment of all the realizability conditions of Vreman et al. [32]. Yet, this does not mean commutation errors reducing filters should not be used, it means that the high-order ones should not be used in conjunction with subgrid-scale models prescribing the generalized turbulent kinetic energy defined in [6] to be positive. After these considerations, up to the date and to our knowledge, there are no discrete filters able to reproduce all the properties of convolution

filters with a reasonable computational cost and thus allowing for a totally consistent discretization of the LES equations with explicit filtering in the literature.

Another well-known context in which filters are used in CFD is the calculation of closures in simulations of turbulent flow with sub-grid scales models like the dynamical procedure [7], the global dynamical procedure [18, 35] or the variational multi-scale methodology [11]. These are widely employed techniques in which the filter performance has a noticeable influence on the overall results but where commutation errors don't play the important role described in the preceding paragraph. In this context, for example, the top hat filter is used to compare subgid scales models on a turbulent mixing layer flow in Vreman et al. [33]. Still in LES, spatial filters are also used in regularization models [30, 25], where filters should verify [26] specific properties.

Filters are also commonly employed in simulations with steep body forces. In these cases, filtering is used to prevent the growth of wiggles produced by large body force gradients [2, 16]. Filtering is also used for similar reasons on simulations of compressible flow with shock waves [1].

In practice, most of the current CFD discrete spatial filtering technology derives from the work of Germano [5],where a convolution filter kernel is found to be the Green function of a second order differential equation and the fundamentals to approximate other low-pass convolution-based filters (e.g. the Gaussian filter) by means of the solution of differential elliptic equations on filtered fields $\hat{\phi}$ are set. This enables computationally affordable approximations to convolution filters in a discrete variables framework, but the resolution of an implicit system of linear equations is required to obtain discrete filtered fields $\hat{\boldsymbol{\phi}}$ from the unfiltered ones $\boldsymbol{\phi}$. Sagaut and Grohens [23] applied filter kernels to Taylor approximations of the unfiltered fields to construct explicit discrete filters for arbitrary meshes. These filters were compared to their theoretical continuous equivalents and tested both on ideal von Karman spectra and within 3D eddy-viscosity LES. Results showed that filter parameters remarkably affect LES results. Vreman et al. [32] approached filters for LES from the models properties. It was shown that only positive filters achieve turbulent sub-grid tensors that always reduce kinetic energy. Vreman [31] later demonstrated that normalized conservative filters can be constructed on non-uniform meshes. To do this, he showed that the adjoint operators of normalized filters are conservative and vice versa. Then, he provided a formula to construct conservative and self adjoint operators from normalized ones and announced two smoothing properties of filters: kinetic energy dissipation and global extrema reduction. More recently, Trias et al. [25] constructed discrete explicit filters fitted for regularization models. In the field of compressible flow simulations, Engquist et al. [3] developed and tested a non-linear filter methodology to capture shocks with conservative adaptative filters and provided a proof of convergence to the weak solution of the original Euler equations. However, the constructed non-linear solution-depending filters entangle filtering and the wiggle detection problem; adding complexity and increasing filter computation time. Also in the compressible flows field, Bogey et al.[1] used a high-order conservative filter to avoid wiggles growth and an adaptative conservative second-order filter at the shock

waves. With it, they simulated shock-vortex interactions and shown the capabilities of this methodology to resolve computational aeroacoustics problems. From the results, it is seen that the adaptative filter does not affect low frequency scales on 1D problems on uniformly spaced structured meshes.

The authors notice that there is, in the literature, a wide range of applications for which the properties that filters should verify to be well fitted for differs. Analytical convolution filters are appropriate for all purposes requiring a constant filter width. However, for analytical or discrete filters approximating the effect of convolution filters, some of its properties are mutually exclusive or lost. For example, adaptative kernel filters do not exactly commute with differentiation. Then, depending on the application, discrete filters in the literature have different properties. As there is no agreement about a minimum set of properties that discrete filters should satisfy in order to be considered filters, there is also confusion about if a discrete operator is really a filter or not. For example, in Finite Volumes (FV) simulations with steep volumes size variations, some of the existing filters can locally "sharpen" fields.

The main objectives of this work are identifying the main properties of filtering, defining discrete filters as operators in concordance with them and providing constraints ensuring their fulfillment. The reader will notice that we neither consider local accuracy to continuous operators a fundamental property of discrete filters nor suppose any set of governing flow equations. This is because the accent is put on bringing the global properties of analytic filtering to discrete spaces and not to any specific application described above. From our point of view, once a spatial discretization is performed, discrete properties of the discrete operators, filters among them, should be derived and/or accomplished in the discrete space. Continuous properties of continuous operators should be translated into discrete properties of discrete operators and not to discrete approximations to continuous operators for which some continuous property is true. Of course, local errors due to discretization are important on simulations that reproduce continuous physics. But as has been shown by Verstappen and Veldman [29], Rozema et al. [21], Trias et al. [**?**] and other authors, preserving operator symmetries rather than making good local approximations can lead to important improvements and better understanding of physics in the CFD science. Using these methods has enabled a better understanding of the physics of fluid flow. For example, Lehmkuhl et al. put them in practice in [12] and captured a low frequency phenomenon affecting a Laminar Separation Bubble (LSB) at the limit layer of a circular cylinder under uniform flow at Reynolds number 3900. The LSB phenomenon is correlated to two different near-wake modes leading to scattering of the results in the literature. Such low-frequency phenomena are sensitive to the numerical discretization to the point that only non dissipative methods can capture them with reasonable mesh refinements.

To reach our purposes, in section 2 we first discuss the analytical convolution filter and its properties. Then, other analytical models of filters are gathered. In the same section, the constraints that make discrete spatial filters satisfy the properties of the convolution filter are detailed. Among the properties, local extrema and total variations evolutions are studied alongside with entropy consistency. Their accomplishment leads to restrictions on local filter strength

(filter width). After that, three filters respecting the imposed constraints are presented in Section 3. In Section 4 it is tested if the proposed filters together with some of the existing in the literature satisfy the aforementioned properties. This is done by means of the eigenvectors of the graph Laplacian matrix that is introduced in Section 2. Tests regarding spatial accuracy are carried out on a singularity field and on an isentropic vortex. Finally, conclusions and possible extensions of the present work are provided in Section 5.

2. Conditions for Adaptive Filtering

For the rest of the document, we use sans serif capital letters to denote matrices, bold letters to denote vectors and calligraphic letters to denote operators. The hat symbol is used to denote filtered field. Plain letters denote scalars. With this, $\hat{\phi}(\boldsymbol{x}) = \mathcal{F}(\phi(\boldsymbol{x}))$ and $\hat{\boldsymbol{\phi}} = \mathsf{F}\boldsymbol{\phi}$. Elements of arrays relative to the control volumes are identified with subscripts "o", "p" and "q" . Elements of matrices establishing relationships between arrays relative to control volumes are identified with two separated subscript indexes "$o\,p$" and the element of the oth row and pth column of a F matrix is denoted with the matrice's letter in minuscule ,i.e., $f_{o\,p}$. Elements of arrays corresponding to interfaces between control volumes are identified with the underlined letters "$\underline{op}$" of the two adjacent control volumes. This notation, together with other symbols whose meaning will be described at first appearance, is used for the rest of the document.

2.1. The Analytical Convolution Filter

Most of the theory on filters for CFD has been derived as a part of the LES theory, where filtering is generally approximated as a convolution operation. Following the notation used in [24]:

$$\hat{\phi}(\boldsymbol{x}) = G \star \phi(\boldsymbol{x}) = \int_{\Omega} K_C(\boldsymbol{x} - \boldsymbol{\xi})\phi(\boldsymbol{\xi})\, d\boldsymbol{\xi}, \tag{1}$$

where ϕ is a generic function, K_C is the filter kernel and is related to the cutoff scales (characteristic of the filter) through a filter characteristic width. The kernel functions K_C of convolution filters are compact supported or rapidly decaying and normalized, i.e. $\int_\Omega K_C(\boldsymbol{\xi})\, d\boldsymbol{\xi} = 1$. Normalization and conservation, i.e. $\int_\Omega \phi\, d\boldsymbol{\xi} = \int_\Omega \hat{\phi}\, d\boldsymbol{\xi}$ are equivalent for convolution operators. Moreover, these filters commute with differentiation and are not dispersive. Additionally, convolution filters can smoothen fields, i.e. be dissipative. This last point is disputed because filtering can also be regarded in the sense of eliminating high Fourier frequencies. Taking into account the applications of filters in CFD and considering that the dissipative property is necessary to smoothen sharp fields, it is not contrary to the LES model and it is in agreement with the realizability conditions in [32], we conclude that dissipation is a commonly necessary property of filters for CFD. Unfortunately, dissipation is not always measured in the same way and, thus, some operators can be considered dissipative according to one criterion while they are not according to another. To us, dissipating is equivalent to reducing a norm on a field gradient and avoiding growth of local maxima and decrease of local minima. If "local" means a ball of radius the support of

K_C, normalized positive, i.e. $K_C \geq 0$, filters with compact support verify the first property for all bounded test functions (see [31]). If the filter kernel is not compact supported, the accomplishment of the first property depends on the test functions. For the second property we use the Total Variations Diminishing on the p norm (TVD_p) criterion to quantify the reduction of gradient norm:

Taking the p norm $||\cdot||_p$ of a function ϕ

$$||\phi||_p = \left(\int_\Omega |\phi|^p d\xi\right)^{1/p}, \tag{2}$$

assuming that $\nabla\phi$ exists and $|\nabla\phi|$ is bounded (this is true for fluid magnitudes), the Total Variations of order p (TV_p) o an operator $\mathcal{F}$ on ϕ is defined as

$$TV_p(\mathcal{F},\phi) = ||\nabla\mathcal{F}(\phi)||_p - ||\nabla\phi||_p. \tag{3}$$

If $TV_p(\mathcal{F},\phi) \leq 0$ for all ϕ, then we say that $\mathcal{F}$ is TVD_p. If $\mathcal{F}$ is a convolution filter with kernel K_C, using Young's inequality $||\nabla\hat{\phi}||_1 \leq ||\nabla\phi||_1 \cdot ||K_C||_1$. If the filter is positive, $||K_C||_1 = 1$ by virtue of normalization. Then, $||\nabla\hat{\phi}||_1 \leq ||\nabla\phi||_1$, so $\mathcal{F}$ is TVD_1. For non positive convolution filters like the spectral cutoff, $||K_C||_1 > 1$ and Young's inequality does not imply TVD_1.

2.2. Other Analytical Filter Models

The following analytical filter models (4-8) justify discrete approximations of (1) in the literature. However, they do not fulfill all of its properties, e.g. commutation with differentiation is lost in all of them. A detailed analysis of all the properties of each model is out the scope of this paper and is not carried out here. They are included to allow for a smooth and more comprehensible transition from (1) to the discrete filters.

The differential filter described in Germano [5] is defined by

$$\phi = (1 - \frac{\bar{\Delta}^2}{24}\nabla^2)\hat{\phi}, \tag{4}$$

where $\bar{\Delta}$ is the filter width. It corresponds to (1) if an exponential filter kernel is used. Using (4) is, for simulations with a large number of nodes, less computationally costly than using (1).

In some cases, the filter cutoff length should vary in space or according to some dependence on the simulated evolving flow. Such adaptability can be obtained by means of the more general class of kernel filters:

$$\hat{\phi}(\boldsymbol{x}) = \int_\Omega K_G(\boldsymbol{x},\boldsymbol{\xi})\phi(\boldsymbol{\xi})\, d\boldsymbol{\xi}. \tag{5}$$

If the filter kernel vanishes sufficiently fast, (5) can be locally approximated taking truncated Taylor series of $\phi(\boldsymbol{\xi})$ near $\boldsymbol{x}$.Thus, one gets explicit polynomial approximations to kernel filters (see [23]):

$$\hat{\phi}(\boldsymbol{x}) \simeq \phi(\boldsymbol{x}) + \sum_{i_1+i_2+i_3=1}^{i_1+i_2+i_3=p} \frac{\partial^p\phi}{\partial^{i_1}\xi_1\partial^{i_2}\xi_2\partial^{i_3}\xi_3}(\boldsymbol{x})\frac{\int_\Omega K_G(\boldsymbol{x},\boldsymbol{\xi})\xi_1^{i_1}\xi_2^{i_2}\xi_3^{i_3}d\boldsymbol{\xi}}{i_1!i_2!i_3!}. \tag{6}$$

As convolution filters are a subspace of kernel filters, (6) can also be applied to approximate those. It is common in all the models considered so far to take filter kernels with vanishing odd moments. Then, only elements with even $i_1+i_2+i_3$ remain in (6). In such case, higher-order differential approximations improve "scales" separation (the scales concept is developed in Section 2.8) as it is shown in [17]. However, as higher-order differential operators can be built by composition and linear combination of the second-order ones, we restrict our analysis on differential filters to those of second order. Thus,

$$\hat{\phi}(\boldsymbol{x}) = (1 + \left(\mathsf{A}(\boldsymbol{x})\bar{\Delta}(\boldsymbol{x})^2\nabla^2\right))\phi(\boldsymbol{x}). \tag{7}$$

When $\mathsf{A} \succeq 0$, i.e., it is a positive semidefinite matrix, and $\mathsf{A}(\boldsymbol{x})\bar{\Delta}^2(\boldsymbol{x})$ is limited to take into account the 2nd law of thermodynamics, this model can be regarded as a time integration step of an unsteady heat conduction problem in an anisotropic material. For the heat conduction problem, moduli of gradients of ϕ should be reduced. This is in accordance with the realizability condition on the convolution filters in [32], with what has been discussed above about the dissipation property of convolution filters for CFD and in consonance with a remark about the differential model (4) in [5]:"we notice that the Gaussian filter corresponds in some sense to a diffusive process of the original function (...)". In the case of (**??**) the limitation on $\mathsf{A}(\boldsymbol{x})\bar{\Delta}^2$ that makes the filter diffusive depends on the values taken by the second derivatives of ϕ or, in other words, (**??**) is conditionally diffusive. This contrasts with the fact that positive convolution filters (1) are dissipative for all ϕ. Moreover, "Germano's" differential filter (4) can not be written in the form of (7) and is therefore essentially different from these. "Germano's" differential filters are inconditionally diffusive because they are equal to (1) with exponential positive kernels.

For isotropic filters or meshes, Equation (7) reduces to

$$\hat{\phi}(\boldsymbol{x}) = (1 + \left(\alpha(\boldsymbol{x})\bar{\Delta}(\boldsymbol{x})^2\nabla^2\right))\phi(\boldsymbol{x}) \tag{8}$$

and the approximation described in Sagaut [23] is recovered. Again, a restriction on $\alpha(\boldsymbol{x})\bar{\Delta}^2(\boldsymbol{x})$ should be imposed for the sake of consistency with the 2nd law of thermodynamics.

Filters based on (1) can separate scales of a field better than those based on (4), (6), (7) or (8). The last three models introduce diffusion to all scales but are more flexible on complex geometries and can be easily applied on both structured and unstructured meshes. On account of this reason and the fact that higher-order filters with better scale separations properties can be built from them, in the following we study discrete versions of (7) and (8).

2.3. Discrete Filter Properties

Let $\mathcal{F}(\cdot) : \mathbb{R}^n \mapsto \mathbb{R}^n$ be a discrete filtering operation with $\hat{\boldsymbol{\phi}} = \mathcal{F}(\boldsymbol{\phi})$. Then, for all $\boldsymbol{\phi}$ and depending on its application, the following properties derived from the approximations (7) and (8) of (1) are usually required:

P-1 Filtering is a local, linear and explicit operation.

P-2 Normalization: Filters do not alter constant fields. $\mathcal{F}(\mathbf{1}) = \mathbf{1}$.

P-3 Conservation: Filtering preserves the integral of $\boldsymbol{\phi}$ on its domain.

P-4 Variations reduction: Filters reduce variations, maxima and/or minima.

P-5 Low dispersion between modes of a mesh.

From the above properties, it is remarkable that P-1, P-2, and P-4 apply to all situations and are intimately related to the continuous concept of low-pass filter while P-3 and P-5 depend on the filter purpose. For example, conservation is not regarded as strictly necessary on test filters of dynamic eddy-viscosity models and low dispersion is not wanted for filters on steep gradient forces, where filtering is performed to transport magnitudes from "small scales" to "larger scales" of meshes.

In the following paragraphs, we explain each property and observe its consequences. We focus our analysis on FV discretizations, extensions to FD or Finite Elements Methods (FEM) are straightforward.

2.4. Filtering is a local, linear and explicit operation [P-1]

Filtering is not a main operation of the NSE, it appears as a CFD tool. Hence, for computer performance and analysis simplicity reasons, and according to the analytic convolution filter and all the other filter models of Section 2.2, linear explicit filters are preferred to others. Then, $\hat{\boldsymbol{\phi}} = \mathsf{F}\boldsymbol{\phi}$.

Since the differential operators of Equations (7) and (8) are local and have compact domains, and for computer performance reasons, filter matrices should be sparse. Accordingly, $f_{op} = 0$ except for $p \in \ N_o = \{p_1, p_2, ..., p_m\}$ neighborhood of the o_{th} cell or for $p = o$. This property also corresponds to models of Equations (1) and (5) with compactly supported kernels.

2.5. Normalization: Filters do not alter constant fields [P-2]

In agreement with the analytical models and because other possibilities don't seem to have any interest for CFD, linear explicit filters should obey

$$(\mathsf{F} - \mathsf{I})\mathbf{1} = \mathbf{0}. \tag{9}$$

In such case, we say that the filter is normalized.

2.6. Conservation [P-3]

Conservation is the basic principle from which the NSE are derived and the main reason why in some applications FV discretizations are preferred over other possibilities such as FD or FEM. In some simulations, magnitudes affected by conservation equations are filtered to improve stability and/or avoid wiggles. Then, they should be conserved in order to preserve the overall method physics. For example, when filtering the body forces applied at some control volumes by an actuator line model of a turbine on a simulation of wind turbine wakes [27],

non conservative filters lead to an imbalance between the turbine model power extraction and the energy change in the free stream. Conservation

$$\int_{\Omega} \hat{\phi}\, \delta\Omega = \int_{\Omega} \phi\, \delta\Omega \tag{10}$$

is true for analytical convolution filters and models (7) and (8).

Defining Ω as the diagonal matrix with the cell volumes at the diagonal elements, one gets the discrete version of (10):

$$\mathbf{1}^T \Omega \hat{\boldsymbol{\phi}} = \mathbf{1}^T \Omega \mathsf{F} \boldsymbol{\phi} = \mathbf{1}^T \Omega \boldsymbol{\phi} \tag{11}$$

Thus,

$$f_{o\,p} = \frac{\Omega_p}{\Omega_o} f_{p\,o} \tag{12}$$

This can also be written as

$$\Omega \mathsf{F} = (\Omega \mathsf{F})^T \tag{13}$$

Notice that the volumes of two neighbor cells are not necessarily equal on general meshes ($\Omega_o \neq \Omega_p$). Hence, for conservative filters $f_{o\,p} \neq f_{p\,o}$ at non-diagonal elements. Consequently, filter matrices have a skew-symmetric part and transport energy between "scales" of the mesh.

Conservation can be relaxed in some applications and non-conservative filters are also useful. For example, test filters used in eddy viscosity methods are not necessarily conservative to keep overall method conservation properties. Among non-conservative filters, the symmetric ones $\mathsf{F} = \mathsf{F}^T$ attract special attention because the aforementioned transport is avoided.

2.7. Variations reduction [P-4]

Roughly speaking, filtering aims at the smearing of maxima and minima and the reduction of variations. This feature has been already discussed for the analytical filters considered in this work and should be imposed on discrete filters by means of an appropriate condition. However, to the best of our knowledge, there is not a clear general consensus about what is the exact computationally affordable condition that represents smearing of discrete fields. We also have noted that not all filters in the literature necessarily fulfill this property for all input fields. For example, the conservative filters introduced in [1] are shown to damp over a range of wavelengths but their behavior on singularity fields, i.e. fields vanishing at all cells excepting one, is not considered. Next, various variations reduction alternatives are discussed.

2.7.1. Local Extrema Diminishing

Local Extrema Diminishing (LED) ensures that if at a certain point $\phi_o > \phi_p \quad \forall p \in N_o$, after filtering: $\hat{\phi}_o = \phi_o + \sum f_{o\,p}(\phi_p - \phi_o) < \phi_o$. Changing the directions of inequalities, the same is true for minima. In the literature, LED is often assumed for all meshes and for all input fields because all $f_{o\,p}$ are

commonly positive by construction. For normalized filters, the necessary and sufficient conditions to fulfill this property are (see [13] and [32]):

$$f_{o\,p} \geq 0 \quad \forall o\,p \tag{14}$$

and

$$f_{o\,o} = 1 - \sum_{p \in N_o} f_{o\,p} \geq 0 \quad \forall o. \tag{15}$$

LED is more restrictive than a bound on the $\mathcal{L}^\infty$ norm of fields. However, in the case of adaptative filtering with filters driven by complex combinations of variables or in the case of non-uniform meshes, LED is not restrictive enough and does not necessarily prevent filters from generating new extrema. Filters that can generate new extrema are not consistent discretizations of the physically consistent analytical models. To illustrate this, we provide the following example:

On the irregular 1D depicted in Figure 1, the volume of i is 1 while the volume of all the other cells is $\omega < 1$. A $\boldsymbol{\phi}$ field evaluating $\phi_i = 1$, and 0 elsewhere is filtered with a one-neighbor stencil LED conservative filter. Since the filter is conservative, according to (12), the values of the filtered field are $\hat{\phi}_i = 1 - 2f$, $\hat{\phi}_{i\pm1} = f/\omega$ and $\hat{\phi}_q = 0$ for other cells, where the scalar f is the filter strength parameter. LED (14), (15) imposes $f \geq 0$, $1 - 2f \geq 0$ and $1 - f/\omega \geq 0$. Then, $0 \leq f \leq min(1/2, \omega)$.

With $\omega = 0.25$ as in the figure, for example, the maximum f allowed by LED is $f = 0.25$. Using it, the values of the filtered field are $\hat{\phi}_i = 0.5$ and $\hat{\phi}_{i\pm1} = 1$. In such case, $\hat{\phi}_{i\pm1} > \hat{\phi}_i$, so the filter would increase the number of maxima (2 after filtering 1 before filtering). This result would break the heat equation interpretation of (8) and (7). For consistency with the 2nd law of thermodynamics, we impose $\hat{\phi}_i \geq \hat{\phi}_{i\pm1}$. Then, the condition $1 - 2f \geq f/\omega$ is obtained, so $0 \leq f \geq \omega/(2\omega + 1) > min(1/2, \omega)$. Unfortunately, the initial field had to be known prior to establishing the inequality direction of $\hat{\phi}_i \geq \hat{\phi}_{i\pm1}$. In order to be robust and practical, filters should not depend on the field they are applied to.

In the present example, consistency with the 2nd law of thermodynamics can be attained from another point of view. If the total of the variations of the whole field is restricted, i.e. $\sum_{o\,p} |\phi_p - \phi_o| \leq \sum_{o\,p} |\hat{\phi}_p - \hat{\phi}_o|$, the condition for $\hat{\phi}_i$ and $\hat{\phi}_{i\pm1}$ is $2 \leq 2\hat{\phi}_{i\pm1} + 2|\hat{\phi}_i - \hat{\phi}_{i\pm1}|$. This inequality provides 2 possible bounds for f. One is $f < \omega/2(\omega + 1)$ and is dismissed because it violates LED. The other, leads to $f \leq \omega/(2\omega + 1)$. TVD_1, has coincided, in this example, with the restriction obtained imposing $\hat{\phi}_i \geq \hat{\phi}_{i\pm1}$, i.e. it has been equivalent to imposing consistency with the dissipation properties of the analytical models. LED has not. Hence, it becomes apparent that a further condition limiting the growth of maxima and minima is to be imposed, together with LED, on discrete filters in general. TVD_p is discussed next.

2.7.2. Total Variations Diminishing

TV_p has been introduced above. It allows a quantification of the amount of wiggles/oscillation tat a field contains. Diminishing TV_1 with can be related

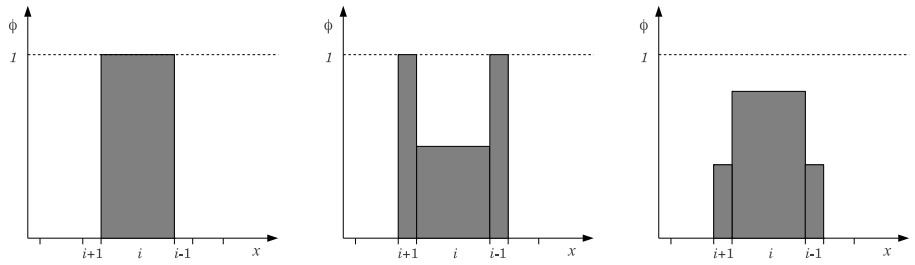

Figure 1: Left: Field values before filtering. Center: Filtered field values obtained with a conservative LED filter. Right: Filtered field values obtained with a conservative, TVD_1 and LED filter.

to the to the differential filter models dissipation properties. In the field of compressible flows simulations, TVD_1 was identified as a sufficient property to construct numerical schemes that don't produce wiggles. First, Harten et al. [9] introduced TVD_1 as an equivalent condition to monotonicity preservation for 1D schemes. The extension of the concept to multiple dimensions was described, for example, in [34]. This extension was made by locally separating the multidimensional problem into various one-dimensional ones by means of a linearization of the equations and enforcing TVD_1 in each direction. This straightforward strategy does not resolve the extension of TVD_1 into multidimensional unstructured grids. Apart from the compressible flow community, TV_1 bounding was also used in image processing technologies (e.g. [22]). However, in filtering literature for CFD it is not explicitly imposed. In our opinion, it is generally accepted that good local approximations of the TVD_1 continuous filters enforce discrete filters to be TVD_1, but according to the results of Section 4 and previous experiences, this assertion is not necessarily true. We consider hereby imposition of the TVD_1 property together with LED on low-pass discrete filters to force consistency with the properties of (8) and (7).

In the compressible flow literature, the usual TV_p norm is the $\mathcal{L}^1$ norm of the graph gradient of a field $||\mathsf{G}\boldsymbol{\phi}||_1$. Where $\mathsf{G} \in \mathcal{M}_{nf\times n}$ (nf is the number of interfaces between cells) is defined as

$$g_{\underline{op}\,r} = \begin{cases} 1 & \text{if} \quad r = p \\ -1 & \text{if} \quad r = o \\ 0 & \text{if} \quad r \neq o \text{ and } r \neq p. \end{cases} \tag{16}$$

The TVD_1 condition on a discrete filter establishes that, for all discrete field $\boldsymbol{\phi}$,

$$||\mathsf{G}\hat{\boldsymbol{\phi}}||_1 = \sum_{\underline{op}} |\hat{\phi}_o - \hat{\phi}_p| \leq \sum_{\underline{op}} |\phi_o - \phi_p| = ||\mathsf{G}\boldsymbol{\phi}||_1. \tag{17}$$

Working with absolute values is cumbersome. Hence, we use the square of the $\mathcal{L}^2$ norm to measure oscillations as it can be written in matrix notation. We obtain

$$2(||\mathsf{G}\hat{\boldsymbol{\phi}}||_2)^2 = \sum_o \sum_{p\in N_o} (\hat{\phi}_o - \hat{\phi}_p)^2 \leq \sum_o \sum_{p\in N_o} (\phi_o - \phi_p)^2 = 2(||\mathsf{G}\boldsymbol{\phi}||_2)^2. \tag{18}$$

We remark that (17) $\not\Rightarrow$ (18) and (18) $\not\Rightarrow$ (17). Now, writing (18) in bilinear form,

$$\boldsymbol{\phi}^T \mathsf{F}^T \mathsf{L} \mathsf{F} \boldsymbol{\phi} \leq \boldsymbol{\phi}^T \mathsf{L} \boldsymbol{\phi}. \tag{19}$$

Where $\mathsf{L} = \mathsf{G}^T \mathsf{G}$ is the graph Laplacian matrix whose elements are:

$$l_{o\,p} = \begin{cases} -1 & \text{if} \quad o \neq p \quad \Omega_p \in N(\Omega_o) \\ 0 & \text{if} \quad o \neq p \quad \Omega_p \notin N_o \\ \overline{\overline{N_o}} & \text{if} \quad o = p. \end{cases} \tag{20}$$

Where $\bar{\bar{\cdot}}$ is the size of a set. In this work, we call L the graph Laplacian matrix or simply the Laplacian matrix. A study of its eigenspace in Section 2.8 shows that it is a good basis for the analysis of the effect of filtering on oscillations.

Condition (19) is also equivalent to

$$\mathsf{K} = \mathsf{L} - \mathsf{F}^T \mathsf{L} \mathsf{F} \succeq 0. \tag{21}$$

Forcing or checking (21) is cumbersome and computationally costly. In Appendix B, its elements are calculated for a general case. Also in in Appendix B, the simpler situation when $f_{o\,p} = \mathcal{O}(\varepsilon)$ with $\varepsilon \to 0$ is studied by means of the Gershgorin circle theorem. Surprisingly to the authors, we could not demonstrate the positive definiteness of K even in this limit case, so the result of the analysis is not conclusive. Nonetheless, inequality (19) can b imposed to the $\boldsymbol{f}_i$ eigenvectors of F. This is equivalent to impose $|\varphi_i| \leq 1$ for all φ_i eigenvalues of F. This can be done applying the Gershgorin circle theorem.

The Gershgorin circle theorem states the eigenvalues of a B matrix lie in $\mathcal{S}_\mathcal{R} \cap \mathcal{S}_\mathcal{C}$ the intersection of the unions of the circles on the complex plane defined as

$$\mathcal{S}_\mathcal{R} = \bigcup_i \mathcal{R}_i \qquad \mathcal{R}_i = \left\{ z \in \mathbb{C} : \, |z - b_{i\,i}| \leq \sum_{j \neq i} |b_{i\,j}| \right\}; \tag{22}$$

$$\mathcal{S}_\mathcal{C} = \bigcup_i \mathcal{C}_i \qquad \mathcal{C}_i = \left\{ z \in \mathbb{C} : \, |z - b_{i\,i}| \leq \sum_{j \neq i} |b_{j\,i}| \right\}. \tag{23}$$

In this case, $|\varphi_i| \leq 1$ is true if, for all o rows of F

$$f_{o\,o} + \sum_{p \in N_o} f_{o\,p} \leq 1 \tag{24}$$

and

$$f_{o\,o} - \sum_{p \in N_o} f_{o\,p} \geq -1. \tag{25}$$

For normalized filters, (24) is always true and (25) is equivalent to (15) because $f_{o\,o} = 1 - \sum_{p \in N_o} f_{o\,p}$.

Conditions (25) and (24) on a filter matrix are necessary but not sufficient to guarantee (18) for all $\boldsymbol{\phi} = \sum_i x_i \boldsymbol{f}_i$. In general, inequality (19) becomes

$$\sum_{i\,j} x_i x_j \boldsymbol{f}_i^T \mathsf{F}^T \mathsf{L} \mathsf{F} \boldsymbol{f}_j \leq \sum_{i\,j} x_i x_j \boldsymbol{f}_i^T \mathsf{L} \boldsymbol{f}_j, \tag{26}$$

which we could not impose for all $\boldsymbol{x}$. However, for filters verifying inequalities (24) and (25) we can speculate that $\exists D \subset \mathbb{R}^n$ such that for $\boldsymbol{x} \in D$ inequality (26) is true. Results in Section 4 confirm its existence.

2.7.3. Entropy Consistency

It seems that TVD_p is a good candidate to control variations of filtering operations to prevent the creation of new maxima and minima. However, the difficulty to ensure it restricts its practical use. To overcome this issue, we propose the Entropy Consistency (EC) condition to achieve variations reduction. To explain this condition, we recall that the studied filters are linear and the superposition principle applies. Now, let $\boldsymbol{e^o}$ be a vector of the canonical basis of fields on a mesh with periodic boundary conditions, i.e. $\boldsymbol{e^o}$'s oth coordinate equals 1 and the rest equals 0. Let F be a filter, hence $\hat{\boldsymbol{e}}^{\boldsymbol{o}} = \mathsf{F}\boldsymbol{e^o}$. If F is such that $0 \leq \hat{e}^o_p \leq 1$ for all p, and all $\hat{e}^o_p$ decrease with some geometric distance to Ω_o so $\hat{e}^o_o \geq \hat{e}^o_p$ for all $p \neq o$, we say that F is EC for $\boldsymbol{e^o}$. If F is EC for all o, we say that F is EC. Applying the superposition principle, EC filters respect the 2nd law of thermodynamics and reproduce a heat conduction problem. Consequently, EC filters smear fields. For a filter to be EC for a $\boldsymbol{e^o}$ vector of the canonical basis it is sufficient that the oth row of F verifies inequalities (27)

$$f_{o\,o} \geq \sum_{p \in N_o} f_{o\,p} \tag{27}$$

and

$$f_{o\,p} \geq 0 \quad \forall p. \tag{28}$$

The interest is on filters that control oscillations for all input fields, i.e. EC filters for which (27) and (28) are true for all o. This is accomplished with positive semidefinite filter matrices with all elements positive. Then, for normalized filters, EC reads

$$1 \geq 2 \sum_{p \in N_o} f_{o\,p} \qquad \forall o, \tag{29}$$

and (28), which is more restrictive than LED. It is straightforward that EC imposes $f_{o\,o} \geq 0.5$. After these conditions and applying the Gershgorin circle theorem, all φ eigenvalues of an EC filter verify $0 \leq \mathbb{R}(\varphi) \leq 1$. On the example of Figure 1, EC gives $0 \leq f \leq min(\omega/2,\, 1/4) \Rightarrow \phi_i \geq \hat{\phi}_i \geq \hat{\phi}_{i\pm1}$.

2.8. Low dispersion between the modes of a mesh [P-5]

Given a mesh and a spatial discretization, if there was a $\mathcal{B} = \{\boldsymbol{b_1}, \boldsymbol{b_2}, ...\boldsymbol{b_n}\}$ orthonormal basis with respect to the euclidean product of $\mathbb{R}^n$ such that it represented oscillations modes of the mesh on which the fields and operators are defined and $i > j \Rightarrow oscillations(\boldsymbol{b_i}) \geq oscillations(\boldsymbol{b_j})$, the oscillations of a vector $\boldsymbol{\phi} = \sum_i x_i \boldsymbol{b_i}$ would be be related to its coordinates on that base. On Cartesian meshes, it is a common practice to use the $\mathcal{B}$ of the Fourier modes. This can not be done on non-uniform meshes where, to the best of our knowledge, there is not an established consensus about which $\mathcal{B}$ is the best solution to account for oscillations. The choice of $\mathcal{B}$ is even less standardized on unstructured meshes because the relation between Fourier modes and mesh modes is

unclear.

A candidate basis that can represent oscillations whatever the mesh is $\mathcal{B}_l = \{\boldsymbol{l_1}, \boldsymbol{l_2}, \boldsymbol{l_3}, ...\boldsymbol{l_n}\}$: the basis of the normalized eigenvectors of the graph Laplacian matrix L defined in (20). Indeed, $\mathsf{L} \succeq 0$ measures oscillations of a field $\boldsymbol{\phi}$ on a spatial discretization and defines a norm on $\mathbb{R}^n$. Taking a pair of eigenvectors $\boldsymbol{l_i}$ and $\boldsymbol{l_j}$ of L corresponding to the eigenvalues λ_i and λ_j, if $|\lambda_i| \geq \lambda_j$, $\boldsymbol{l_i}$ contains more oscillations than $\boldsymbol{l_j}$ and $\boldsymbol{l_i} \cdot \boldsymbol{l_j} = 0$ if $i \neq j$, $\boldsymbol{l_j} \cdot \boldsymbol{l_j} = 1$. Hence, the vectors of $\mathcal{B}_l$ represent of the modes of a mesh. To show this relationship, eigenvectors of L on an structured and an unstructured meshes are depicted, respectively, in Figures 3 and 4. Eigenvalues of L for the same meshes are shown in Figure 2.

Other symmetric positive-definite matrices can be used as a basic norm for measuring oscillations and computing a useful basis to represent mesh modes. Mainly, candidates are expected among discrete differential Laplacian operators or graph Laplacians matrices with volume weightings. Our experience during this work shows that the operator defined in equations (9a-9c) of [19] with centroid as field points also contains information about the mesh distortion and the ϕ fields maxima and minima can be masked by cell volumes changes.

Now, given an endomorphism (a filter matrix) $\mathsf{F} : \mathbb{R}^n \mapsto \mathbb{R}^n$, the effect it produces on the oscillations can be studied by means of the images of each of the vectors of the modes basis. If F was such that $\mathsf{F}\boldsymbol{b_i} = \beta_i \boldsymbol{b_i}$, with $\beta_i \in \mathbb{R}$, we would say that F does not produce dispersion because variations on oscillations modes would be independent. Unfortunately, F generally projects $\boldsymbol{b_i}$ on more vectors of $\mathcal{B}$ than itself. This could be resolved changing the basis on which the analysis is performed, but then the basis might not represent oscillations. Changing the coordinates with the $\Omega^{-1/2}$ matrix, one gets a symmetric filter matrix from a conservative filter. Then, the corresponding change on L would break its symmetry and its capacity to measure oscillation would be lost. Still, one could use $\mathsf{F}' = \Omega^{1/2}\mathsf{F}\Omega^{-1/2}$ the symmetric filter matrix on the new basis as oscillations norm. Then, its eigenvectors would be mesh modes and no dispersion would occur; but these properties would be true on a space where variables have $\Omega^{-1/2}$ dimensions and returning to the physically relevant space would break them. Hence, we stick to an oscillations measuring matrix and its associated basis and we say that filters that project $\boldsymbol{b_i}$ on other vectors of $\mathcal{B}$ than itself are dispersive. Note that if F is symmetric in the physically relevant space, then it can define the oscillations norm and $\mathcal{B}$, so dispersion would not occur.

Regarding the analytical filter models of Section 2.2 and taking Fourier series, adaptative filters are dispersive while non adaptative ones are not. Still, we consider that transporting oscillations from low modes to high modes is a negative filtering behavior but, as we could not deduce proper constraints to avoid it and it does not disagree with adaptative filters, no further actions than observations are taken in this sense.

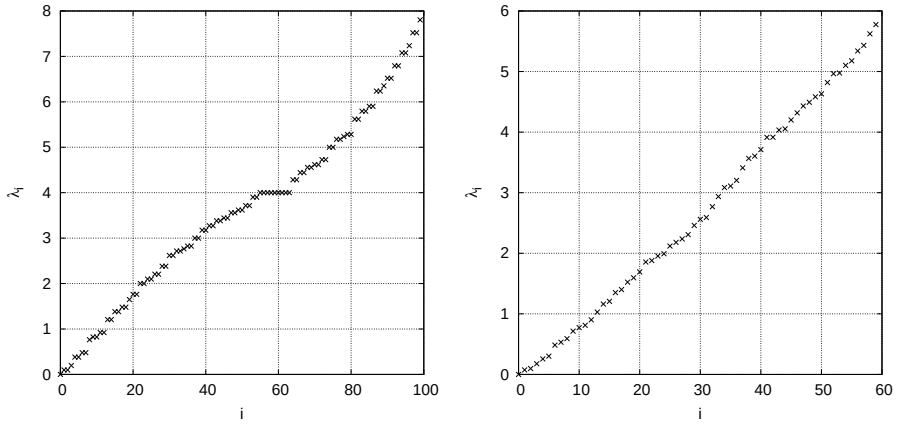

Figure 2: Eigenvalues of L on the structured mesh1 (left) and the unstructured mesh2 (right) of Section 4.

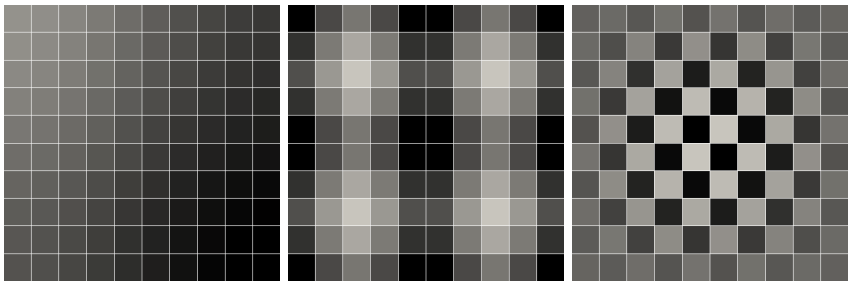

Figure 3: Eigenvectors of the Laplacian matrix on the structured "mesh1" of Section 4. From left to right: 2, 15, 99.

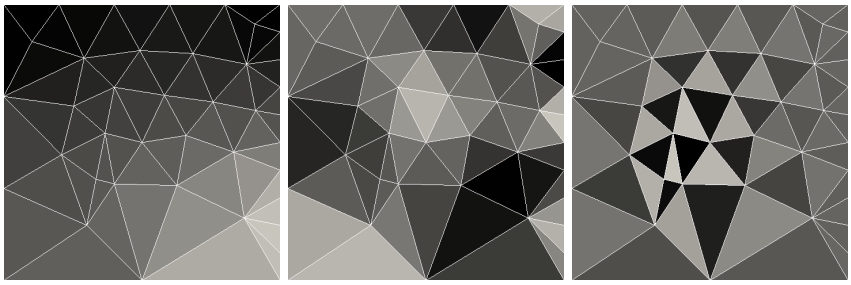

Figure 4: Eigenvectors of the Laplacian matrix on the unstructured mesh "mesh2" of Section 4. From left to right: 2, 12, 59.

3. Limited Filters for CFD

In this section, a set of filters accomplishing some of the conditions introduced in Section 2 on cell-centered FV discretizations are presented. Extensions to other discretizations can be envisaged.

3.1. Conservative Limited Filter (CLF)

A normalized conservative filter F for $\phi \in \mathbb{R}^n$ has $\sum_o \overline{\overline{N_o}}/2$ independent dimensionless $f_{o\,p}$ elements. As it has been shown in Section 2.6, $\check{\mathsf{F}} = \Omega\mathsf{F}$ is symmetric. We write $f_{o\,p} = \check{f}_{o\,p}/\Omega_o = g_{o\,p}\Omega_{\underline{op}}/\Omega_o$ where $\Omega_{\underline{op}}$ is a function of the volumes of cells o and p. For consistency, $\Omega_{\underline{op}}(\Omega_o, \Omega_p) = \Omega_{\underline{po}}(\Omega_p, \Omega_o)$. There is laterality in the definition of $\Omega_{\underline{op}}$. For example, Trias et al. [25] chose $\Omega_{\underline{op}}$ to be the volume of the staggered cells. We use $\Omega_{\underline{op}} = \sqrt{\Omega_o\Omega_p}$ for simplicity and the freedom to use vertex-connected neighbors, which cannot be easily done with staggered cells constructions.

Now, supposing an input set of $g_{o\,p} \geq 0$ for all o and p, LED or EC can be granted by means of two different procedures: The first procedure consists of scaling the $g_{o\,p}$ input values only if

$$Sg_o = \sigma \sum_{p \in N_o} f_{o\,p} = \sigma \frac{1}{\Omega_o} \sum_{p \in N_o} \Omega_{\underline{op}} g_{o\,p} > 1. \tag{30}$$

In that case all $\{g_{o\,p} : p \in N_o\}$ are divided by Sg_o. The second procedure consists of bounding all $g_{o\,p}$ with

$$g_{o\,p} \leq min\left(\frac{\Omega_o}{\sigma\Omega_{\underline{op}}\overline{\overline{N_o}}}, \frac{\Omega_p}{\sigma\Omega_{\underline{op}}\overline{\overline{N_p}}} \right). \tag{31}$$

Here, σ is a number that can evaluate 1 or 2. LED is obtained with $\sigma = 1$ while EC is obtained with $\sigma = 2$. Approximation (30) is less restrictive than (31).

Finally, using the normalization equation, $f_{o\,o} = 1 - \sum_{p \in N_o} f_{o\,p}$.

3.2. Differential Limited Filters

Both the Laplacian and the box 2nd order filters from [23] can be expressed, according to equation (8) as

$$\hat{\phi} = \phi + \frac{(\epsilon\Delta)^2}{24}\nabla^2\phi + \mathcal{O}(\Delta^4) \tag{32}$$

where Δ is the characteristic length of a CV and ϵ the dimensionless parameter controlling the filter width. We apply the model of equation (7) instead because it allows adapting Δ and ϵ to each interface. Then, depending on the chosen approximation to the Laplacian operator, conservation and symmetry can be imposed.

We propose a Conservative Differential Limited Filter (CDLF) which is a particularization of CLF:

$$f_{o\,p} = \frac{\epsilon_{\underline{op}}^2(\Omega_o\Omega_p)^{1/3}A_{\underline{op}}}{24\Omega_o(\boldsymbol{r}_{\underline{\boldsymbol{op}}} \cdot \boldsymbol{n}_{\underline{\boldsymbol{op}}})} \quad \text{if } o \neq p \quad ; \quad f_{o\,o} = 1 - \sum_{p \in N_o} f_{o\,p}. \tag{33}$$

And a Symmetric Differential Limited Filter (SDLF):

$$f_{o\,p} = \frac{\epsilon_{\underline{op}}^2 A_{\underline{op}}}{24(\Omega_o\Omega_p)^{1/6}(\boldsymbol{r}_{\underline{\boldsymbol{op}}} \cdot \boldsymbol{n}_{\underline{\boldsymbol{op}}})} \quad \text{if } o \neq p \quad ; \quad f_{o\,o} = 1 - \sum_{p \in N_o} f_{o\,p}. \tag{34}$$

For both cases, $\boldsymbol{r_{\underline{op}}}$ is the vector that goes from the center of cell o to the center of cell p, $\boldsymbol{n_{\underline{op}}}$ is the unit vector normal to the interface between the cells directed towards p, $A_{\underline{op}}$ is the area between the two cells, and Ω_o is the volume of cell o. The filter width parameter $\epsilon_{\underline{op}}$ is evaluated at interfaces.

To accomplish LED or EC, the elements of the filter matrix should verify $\sigma \sum_{p \in N_o} f_{o\,p} \leq 1$ with $\sigma = 1$ for LED or $\sigma = 2$ for EC. This condition can be attained limiting $\epsilon_{\underline{op}}$ in a similar fashion to what has been done for CLF. Again, there are two different procedures to impose the mentioned limitations: The first, less restrictive than the other, is applied only in the case that $S_o = \sigma \sum_p f_{o\,p} > 1$ at some o cell. If this occurs, using

$$(\epsilon^*_{\underline{op}})^2 = \frac{\epsilon^2_{\underline{op}}}{\overline{\overline{S_o}}} \tag{35}$$

instead of $\epsilon^2_{\underline{op}}$ $\forall p \in N_o$ resolves the problem. The second possibility is to limit all $\epsilon^2_{\underline{op}}$ for all o and for all p so that

$$\epsilon^2_{\underline{op}} \leq \left\{ \frac{1}{\sigma \overline{\overline{N_o}}} \sum_{p \in N_o} \frac{A_{\underline{op}}}{24(\Omega_o \Omega_p)^{1/6} (\boldsymbol{r_{\underline{op}}} \cdot \boldsymbol{n_{\underline{op}}})}, \frac{1}{\sigma \overline{\overline{N_p}}} \sum_{q \in N_p} \frac{A_{\underline{pq}}}{24(\Omega_p \Omega_q)^{1/6} (\boldsymbol{r_{\underline{pq}}} \cdot \boldsymbol{n_{\underline{pq}}})} \right\}. \tag{36}$$

Both schemes approximate $\nabla \cdot (\mathsf{A} \nabla(\cdot))$. As stencils with all vertex-neighbors are not straightforward, we propose a methodology to do this in the following paragraphs.

3.3. Filters with Vertex-Neighbors Stencils

In FV discretizations, the divergence theorem is the most common tool to obtain discrete operators. Least squares approximations of the values of the fields at interfaces would allow the use of vertex-neighbor stencils, but this results in the loss of control on preservation of operator symmetries. To overcome this problem, we propose the use of ghost surfaces connecting each cell to each of its vertex-neighbors and to apply the divergence theorem straightforwardly.

Let $\mathsf{L_g}$ be the discrete geometric Laplacian matrix of a given mesh. Then, for a cell p sharing a face with cell o, $lg_{o\,p} = A_{\underline{op}}/(\Omega_o ds_{\underline{op}})$, with $ds_{\underline{op}} = \boldsymbol{r_{\underline{op}}} \cdot \boldsymbol{n_{\underline{op}}}$. To extend this formula to a "q" cell , vertex neighbor of o, i.e., sharing one v vertex with it, we propose to use

$$A_{\underline{oq}} = \frac{\Omega_o + \Omega_q}{h_{\underline{vo}} + h_{\underline{vq}}} \tag{37}$$

and

$$\boldsymbol{n_{\underline{oq}}} = \begin{cases} \frac{(\boldsymbol{r_{\underline{vo}}} \wedge \boldsymbol{r_{\underline{vq}}}) \wedge (\boldsymbol{r_{\underline{vo}}} + \boldsymbol{r_{\underline{vq}}})}{||(\boldsymbol{r_{\underline{vo}}} \wedge \boldsymbol{r_{\underline{vq}}}) \wedge (\boldsymbol{r_{\underline{vo}}} + \boldsymbol{r_{\underline{vq}}})||} & \text{if} \quad \boldsymbol{r_{\underline{vo}}} \wedge \boldsymbol{r_{\underline{vq}}} \neq \boldsymbol{0} \\ \frac{\boldsymbol{r_{\underline{vo}}}}{||\boldsymbol{r_{\underline{vo}}}||} & \text{if} \quad \boldsymbol{r_{\underline{vo}}} \wedge \boldsymbol{r_{\underline{vq}}} = \boldsymbol{0} \end{cases} \tag{38}$$

Where $\boldsymbol{r_{\underline{vq}}}$ is the vector from the v vertex to the centroid of cell q and h_{vq} is the volumetric height of the o cell that passes through vertex v, $\boldsymbol{r_{\underline{vo}}}$ and $h_{\underline{vo}}$ are their equivalents for cell o. The value of volumetric heights depends on the

polyhedron types of the cells they are referred to. For example, if o is a tetrahedron, $h_{\underline{vo}} = h_v/3$, with h_v the distance between v and the face of opposed to v. Other polyhedra induce some laterality in the values of $h_{\underline{vo}}$ and $h_{\underline{vo}}$ but satisfactory casuistic solutions can be found.

Equations (37) and (38) are used to extend the introduced filters to vertex neighbors stencils. LED and EC limitations are imposed in the same way as for their face neighbor stencils equivalents.

4. Tests

There is a large variety of tests for filters available in the literature but the properties they are designed to quantify differ appreciably between authors, so comparison of filters developed in different works is not straightforward. For example, the test described in Marsden et al. [15] is designed to study the filter commutation error while tests in Sagaut et al. [23] are designed to compare the discrete filters to their analytic models. Another factor that makes comparisons more difficult is that authors often test 3D filters on full CFD simulations, not isolatedly, so the performance of filters can be accidentally concealed. Following the ideas exposed in the introduction, the tests conducted and reported in this document focus on global properties characterizing filtering. Namely, we propose tests to check the accomplishment of conservation, variations evolution and dispersion properties introduced and developed in Section 2. After that, we conduct tests on a singularity and on an isentropic vortex to study the performance of filter on situations more similar to CFD simulations.

In order to analyze dispersion and to clarify conservation and variations evolution we use the basis of the graph Laplacian matrix according to Section 2.8. In software terms, we used the `gsl_eigen_symmv` routine of the `gsl` library [4] to calculate the eigenvectors of L.

The tested filters are: a Laplacian approximation to a convolution Gaussian filter, a box based filter and the filters developed in Section 3. The Laplacian filter is identified as “Laplacian” and the box as “Box”. Both of them are detailed in Appendix A.

For the tests on the introduced properties, all filters are tested with both adaptative and constant filter width parameters (filter drivers) on two different meshes. We specify the following names code to identify the performed tests:

XXXX(V)-Y-Z

Here, "XXXX“ stands for the filter name; "V“ expresses that the filter uses vertex-neighbor stencils (face-neighbors stencils are assumed by default), "Y“ indicates how the filter driver has been computed and "Z“ identifies the mesh used for the test. The "Y“ parameter can be Constant (C) when the parameter equals 1.5 at all cells, Maxima (M) when it is computed as $|\mathsf{L}\boldsymbol{\phi}|$ or Random (R) when it is has a probability of 0.2 to be different to zero, in which case it is a random number between 0 and 4. The constant filters parameters are common within LES, (M) filter parameters can be used to filter inserted body

forces like in [27] and (R) represents situations similar to shock wave detection and conservative fields filtering (see [1]). Two different 2D meshes respectively identified with 1 and 2 have been used: a uniform structured mesh with 100 CV "mesh1" and an unstructured mesh with 60 CV "mesh2", both have been created with the `ANSYS ICEM CFD` software. These meshes are in practice 3D and 1 CV thick. The thickness of mesh1 is 0.1 while the thickness of mesh2 is $60^{-0.5}$. These thicknesses equalize the characteristic lengths of volumes in all dimensions. All boundary conditions are Neumann: the tested fields evaluate the same at the boundary face nodes than in the cell they are in contact with. Hence, boundary face nodes are neither included in L nor in any F. On mesh1, CDLF and SDLF are identical by construction but results of both are represented in all plots to confirm this statement.

For the tests on singularity fields and the isentropic vortex, only the filter names are necessary and the other parameters are specified in the corresponding sections.

The physical interpretation of the filter strength differs between the studied filters and so does the filtering strength parameters. In order to achieve better comparisons, relationships between filter strength parameters have been deduced so that, for "C" and on uniform meshes, all filters with face stencils produce very similar outputs. These same parameters are also used on the vertex stencils filters counterparts. These relations are also applied on situations with nonuniform meshes or adaptative filters. Further details on filter strengths relationships are in Appendix C.

Filter strength parameters of the filters proposed in Section 3 can be limited using a cell based methodology like in equation (31) or an interface based methodology like in equation (30). Tests on the filters properties have been conducted with both limiting methodologies but, as results are almost indistinguishable, only those with the cell based methodology are included in this paper. Otherwise, tests on the isentropic vortex and the singularity have been conducted with the cell based methodology only.

4.1. Total Variations Evolution Tests

The main objective of a filter is to damp oscillated fields without affecting those with few oscillations. In the basis of the Laplacian matrix, it is damping the $\boldsymbol{l}_i$ with high λ_i while not damping much the others. We denote $\boldsymbol{\lambda}\uparrow$ the vector of eigenvalues of L in increasing order. In Section 2.7 several approximations to damping measurements have been considered. We provide here representations of $||\mathsf{G}\widehat{\boldsymbol{l}_i}||_1/||\mathsf{G}\boldsymbol{l_i}||_1$ vs. i (where each $\boldsymbol{l_i}$ corresponds to a λ_i) as a measure of filter damping performance. For the sake of conciseness and because they are very similar, we only show results obtained with the LED condition and we only comment differences with EC at the end of the analysis.

Overall, after the results obtained with the constant filter driver, all filters damp as pretended: filtering effect grows with i. Focusing on results with mesh1 shown in Figure 5, it appears that, after scaling filter drivers according to Appendix C, all filters except Box give indistinguishable results. Differences

between Box and all the other filters come from the filter driver scaling process, where we did not take into account that boundary cells have lower number of neighbors. Besides, on results with mesh2 shown in Figure 6, it is observed that all filters damp in a similar fashion. In consonance with their formulations, though, results are not equal. However, differences between Box or Laplacian with respect to the newly developed filters are not much bigger than those between Box and Laplacian. Therefore, we consider that the developed filters damp similarly to the previously existing ones provided that the filter parameters are scaled. Finally, for a given filtering parameter, filters with vertex neighbors introduce more damping. This is because of the larger size of vertex stencils is not taken into account when scaling them.

Figures 7 and 8 show the results obtained with "M" filter parameters. All filters give similar results, specially on mesh1. Their transfer functions do not damp for the low oscillated modes ($i \to 0$) and become gradually more aggressive for more oscillated ones ($i \to n$). This behavior fits pretty well with the commonly expected transfer function of low-pass filters. However, none of the studied filters reaches the total elimination of the high modes on any of the tested meshes. With regards to the differences between faces stencils and vertices stencils, what has been described for "C" applies.

Results with the random filter driver are shown in Figures 9 and 10 show that CLF, CDLF and SDLF increase oscillations on both meshes at low i. This negative effect is more evident on mesh 2 and with vertices stencils. As the probability to filter activation is relatively low compared to "C" and to "M" with high i, the damping is lesser. However, all filters tend to reduce oscillation at high i, which is a positive behavior. Among them, CLF, CDLF and SDLF cause the highest damping on most i.

Filters limited with LED are more damping than those limited with EC when the limitation is active. However, damping behaviors are qualitatively the same. The most relevant quantitative differences have been found on the case with mesh2 and "R" pictured on Figure 11 for EC. In this situation, EC approaches better to the reduction of total variations at all modes. Still, at some low modes, total variations increased on the order of 10^{-3} instead of 10^{-2} achieved with LED. Further experiences have been carried with random fields and other settings of the "R" filter driver. The conclusion is that total variations growth has only been observed in situations where the filter driver equals zero at most of the cells while takes values as high as to activate LED or EC at some of them and the base field is a low oscillated mode. This setting is the most effective in the transport of fields from large (test field) to small scales (filter activation field) but it does not correspond to CFD. Some tests without LED nor EC restrictions have been also conducted. Oscillation growth is observed for some $\boldsymbol{b_i}$ with all filters and all meshes when the filter strength parameter is higher than the permitted by LED. We include Figure 12 as an example.

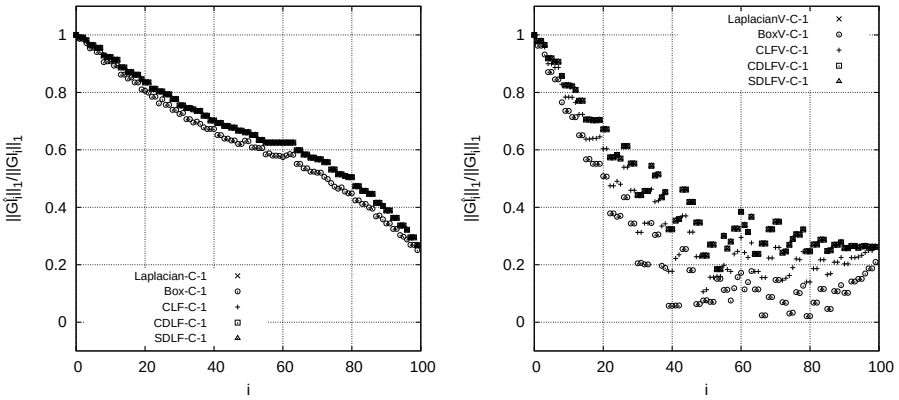

Figure 5: $||G\hat{\boldsymbol{l}_i}||_1/||G\boldsymbol{l_i}||_1$vs. i with the "C" filter driver, mesh1 and LED. Left: faces stencils. Right: vertices stencils.

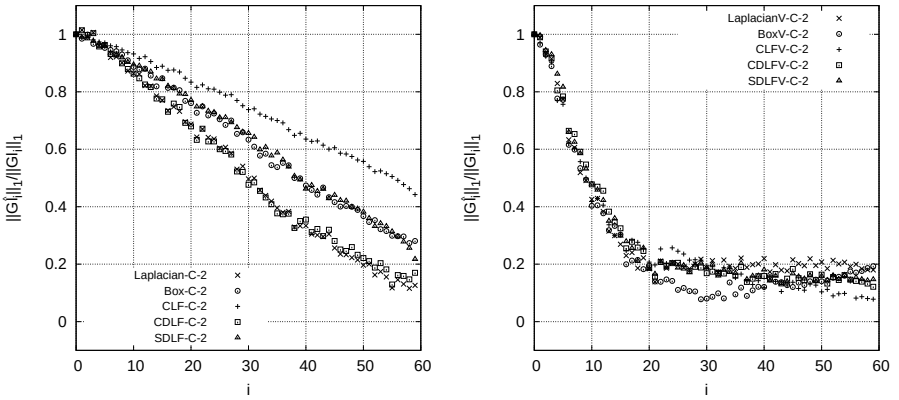

Figure 6: $||G\hat{\boldsymbol{l}_i}||_1/||G\boldsymbol{l_i}||_1$ vs. i with the "C" filter driver, mesh2 and LED. Left: faces stencils. Right: vertices stencils.

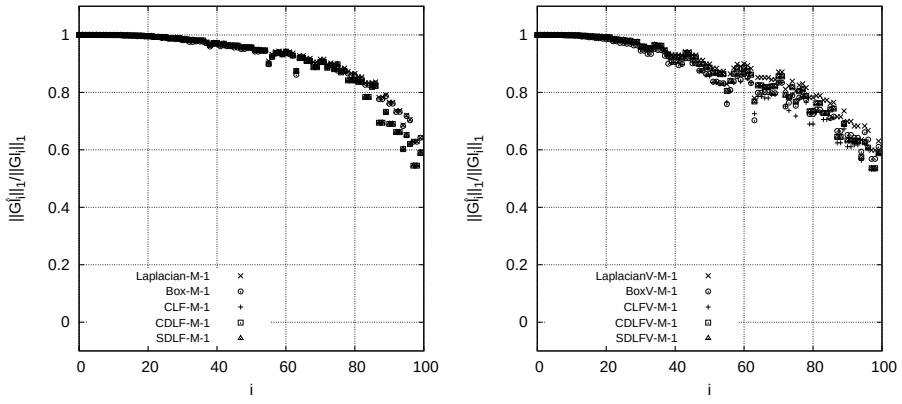

Figure 7: $||G\hat{\boldsymbol{l}_i}||_1/||G\boldsymbol{l}_i||_1$ vs. i with the "M" filter driver, mesh1 and LED. Left: faces stencils. Right: vertices stencils.

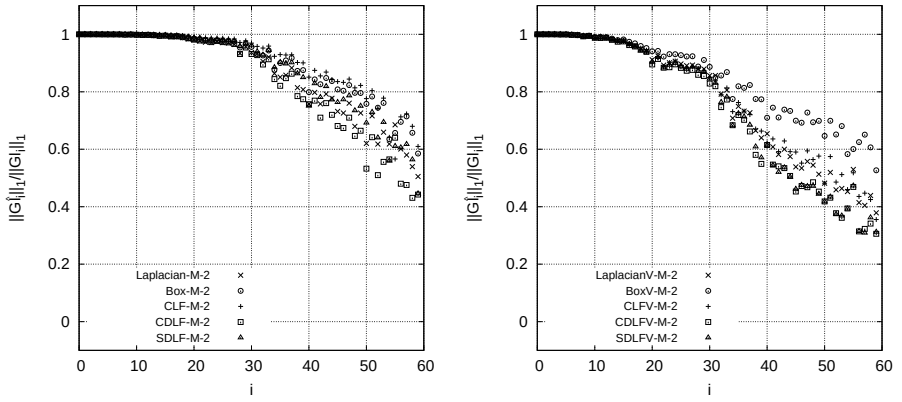

Figure 8: $||G\hat{\boldsymbol{l}_i}||_1/||G\boldsymbol{l}_i||_1$ vs. i with the "M" filter driver, mesh2 and LED. Left: faces stencils. Right: vertices stencils.

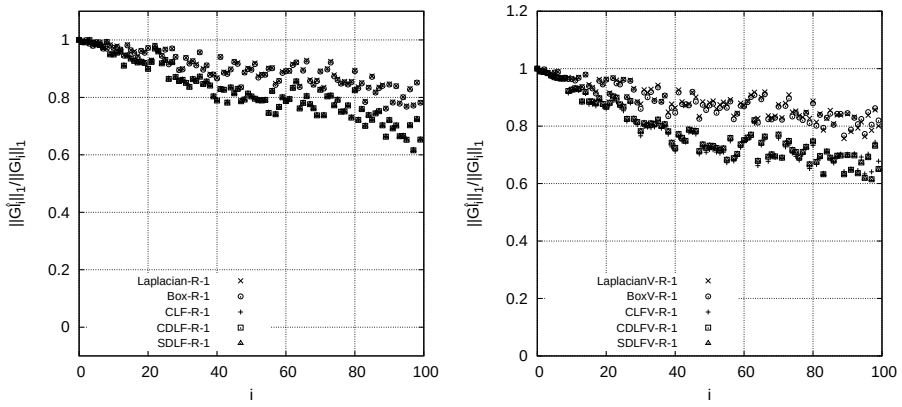

Figure 9: $||\mathsf{G}\hat{\boldsymbol{l}_i}||_1/||\mathsf{G}\boldsymbol{l_i}||_1$ vs. i with the "R" filter driver, mesh1 and LED. Left: faces stencils. Right: vertices stencils.

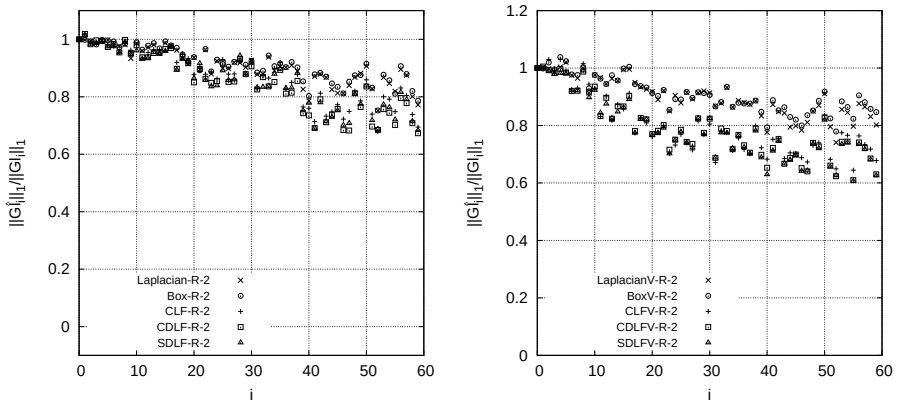

Figure 10: $||\mathsf{G}\hat{\boldsymbol{l}_i}||_1/||\mathsf{G}\boldsymbol{l_i}||_1$ vs. i with the "R" filter driver, mesh2 and LED. Left: faces stencils. Right: vertices stencils.

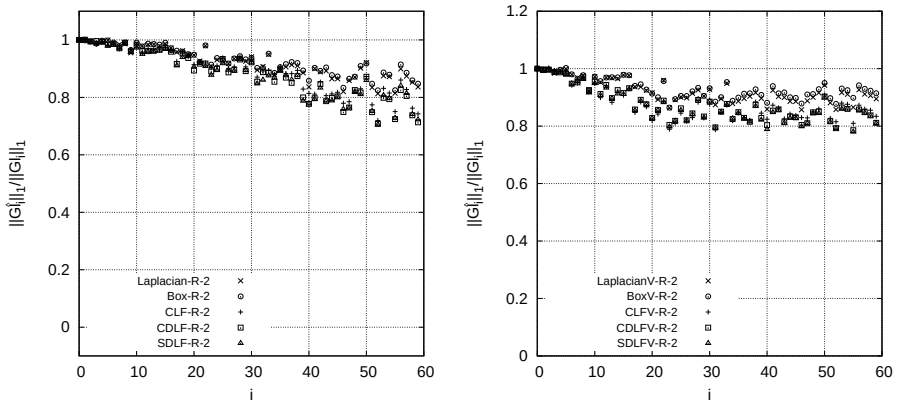

Figure 11: $||\mathsf{G}\hat{\boldsymbol{l}_i}||_1/||\mathsf{G}\boldsymbol{l}_i||_1$ vs. i with the "R" filter driver, mesh2 and EC. Left: faces stencils. Right: vertices stencils.

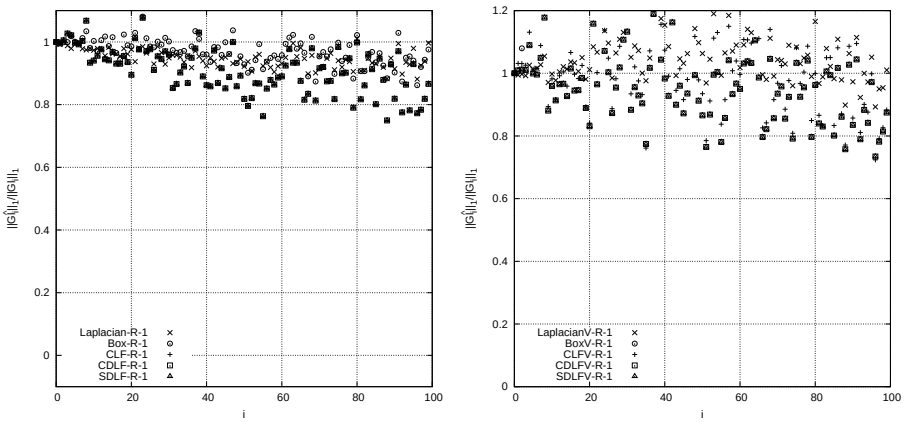

Figure 12: $||\mathsf{G}\hat{\boldsymbol{l}_i}||_1/||\mathsf{G}\boldsymbol{l}_i||_1$ vs. i with the "R" filter driver, mesh1 and no filter strength limit. Left: faces stencils. Right: vertices stencils.

4.2. Conservation Tests

For a conservative filter, the magnitude $\mathbf{1}^T\Omega(\boldsymbol{l_i} - \hat{\boldsymbol{l}}_{\boldsymbol{i}})$ equals zero. Here, its resulting value calculated with the considered filters configurations is analyzed to study possible relations on the oscillations present in the test field. Results with the "C" filter driver are plotted on Figures 13 and 14. On mesh1, only Box is not conservative while on mesh2, only CLF and CDLF conserve the integral of $\boldsymbol{\phi}$ in the domain. It is also observed that vertex-stencils filters are less conservative, probably because they have a greater effect when the filter strength parameter is the same. Results of tests with the "M" filter driver are plotted in Figures 15 and 16. On mesh1, CLF, CDLF and SDLF are conservative for all $\boldsymbol{l_i}$ while Laplacian and Box are remarkably non conservative. On mesh2, SDLF is not conservative anymore but it is closer to it than Laplacian or Box. Again, vertex stencils reduce conservation of non-conservative filters. In all cases, a dependence of $\mathbf{1}^T\Omega(\boldsymbol{l_i} - \hat{\boldsymbol{l}}_{\boldsymbol{i}})$ with respect to i is observed with "M". This can be attributed to the growth of the filter width with i for mesh2, while for mesh1 $\mathbf{1}^T\Omega(\boldsymbol{l_i} - \hat{\boldsymbol{l}}_{\boldsymbol{i}})$ is higher for i around 60. Results of tests with "R" are not reproduced. They differ from those with "M" because there is not a dependence on i.

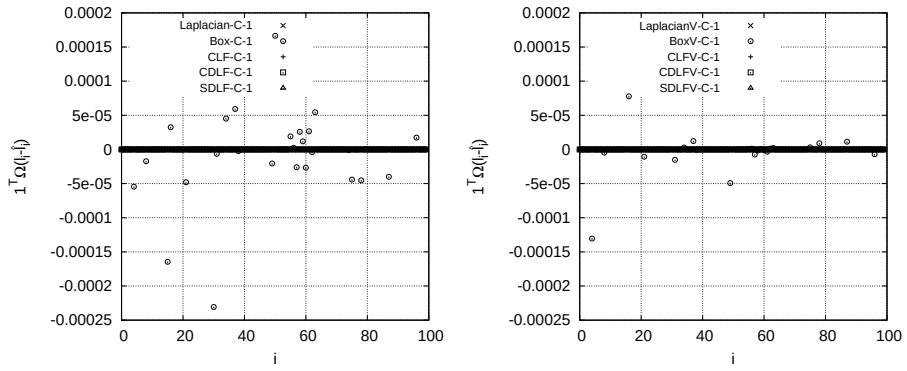

Figure 13: $\mathbf{1}^T\Omega(\boldsymbol{l_i} - \hat{\boldsymbol{l}}_{\boldsymbol{i}})$ vs. i with the "C" filter driver, mesh1 and LED. Left: faces stencils. Right: vertices stencils.

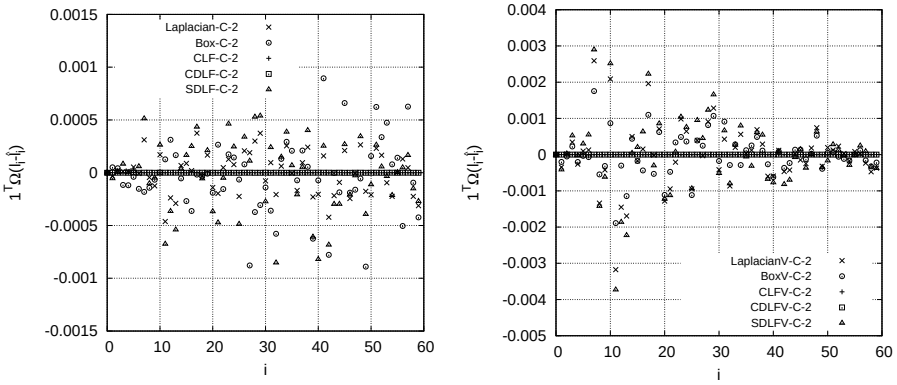

Figure 14: $\mathbf{1}^T\Omega(\boldsymbol{l_i} - \hat{\boldsymbol{l}}_{\boldsymbol{i}})$ vs. i with the "C" filter driver, mesh2 and LED. Left: faces stencils. Right: vertices stencils.

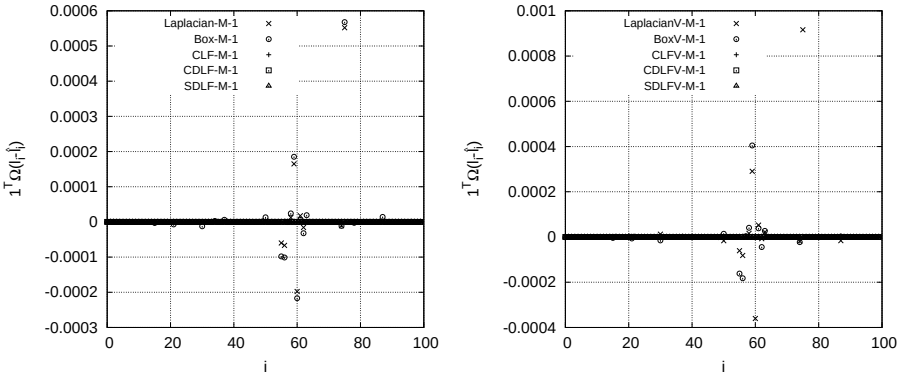

Figure 15: $\mathbf{1}^T\Omega(\boldsymbol{l_i} - \hat{\boldsymbol{l}}_{\boldsymbol{i}})$ vs. i with the "M" filter driver, mesh1 and LED. Left: faces stencils. Right: vertices stencils.

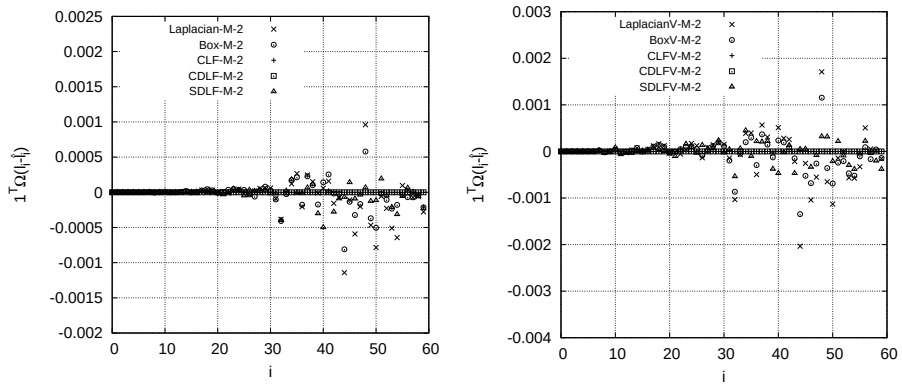

Figure 16: $\mathbf{1}^T\Omega(\boldsymbol{l_i} - \hat{\boldsymbol{l}}_{\boldsymbol{i}})$ vs. i with the "M" filter driver, mesh2 and LED. Left: faces stencils. Right: vertices stencils.

4.3. Dispersion Tests

An analysis focused on the study of the dispersion that a filter produces on each $\boldsymbol{l_i}$ has also been conducted. 2D grayscale plots of the moduli of coordinates of $\hat{\boldsymbol{l}}_{\boldsymbol{i}}$ in the basis $\mathcal{B}_l$ represent the dispersion produced by each filter. For a position $i\,j$ of the graphs in Figures 17-20, the ordinate i represents the filtered mode $\boldsymbol{l_i}$, the abscissa value j represents the index of the coordinate j in $\mathcal{B}_l$ basis, and the gray intensity represents the absolute value of $(\hat{l}_i)_j$ in logarithmic scale. Accordingly, non-dispersing filters produce dark gray in the diagonal and white elsewhere. However, filters transporting energy from higher to lower modes are also considered satisfactory. In the present test, such behavior would cause a dark gray diagonal, a lighter dark gray on the lower right corner and a lighter gray at the other positions. Other criteria like dispersing to close modes (gray only near the diagonal, white at the rest) can also be useful for CFD purposes. Most of the figures that included here contain data obtained with EC restricted filters only. Differences between EC and LED are described at the end of the section.

Results show that the mesh, the filter driver and the stencil have a noticeable influence on the dispersion properties of the filters. Regarding the difference between meshes for a given set of filter, driver and stencil, we notice that, for all situations excepting "R" drivers, filters produce remarkably more dispersion on mesh2 than on mesh1. On mesh1 and given an stencil, Gauss, CLF, CDLF and SDLF are equal. With this mesh, (Figures 17 and 18) and after the results obtained with the "C" and "M" filter drivers, $(\hat{l}_i)_j$ take values different to zero for most i and some j around 60 and for some i around 60 and j. So, the graphs are mostly white and exhibit ordered gray patterns symmetric respect to the diagonal. The eigenvectors $\hat{\boldsymbol{l}}_{\boldsymbol{i}}$ for which more dispersion is observed are the same than those towards which the test fields are mostly projected. They are also the lesser conservative ones with "M" and mesh1 in the conservation test. Figures 19 and 20 show results on mesh2. Only CDLF and Box are represented because differences with other filters are irrelevant in this test. No ordered patterns are

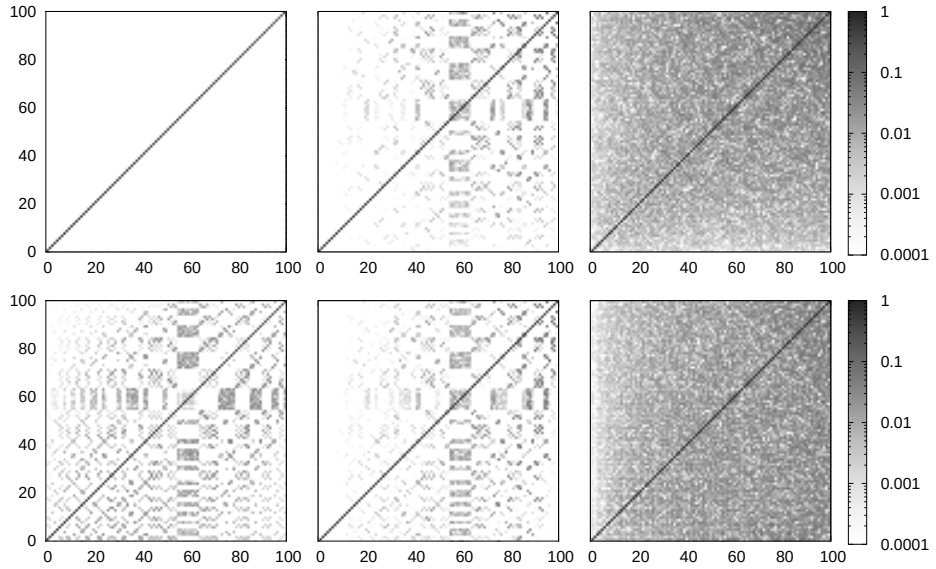

Figure 17: Dispersion tests on mesh1 with faces stencils and EC. Top: CDLF, bottom: Box. Columns, from left to right: C, M, R.

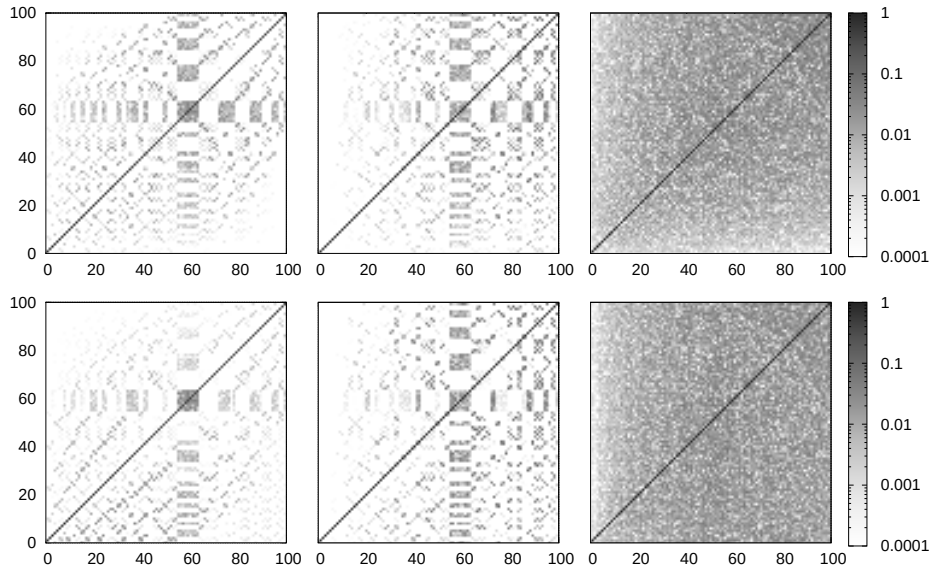

Figure 18: Dispersion tests on mesh1 with vertices stencils and EC. Top: CDLF, bottom: Box. Columns, from left to right: C, M, R.

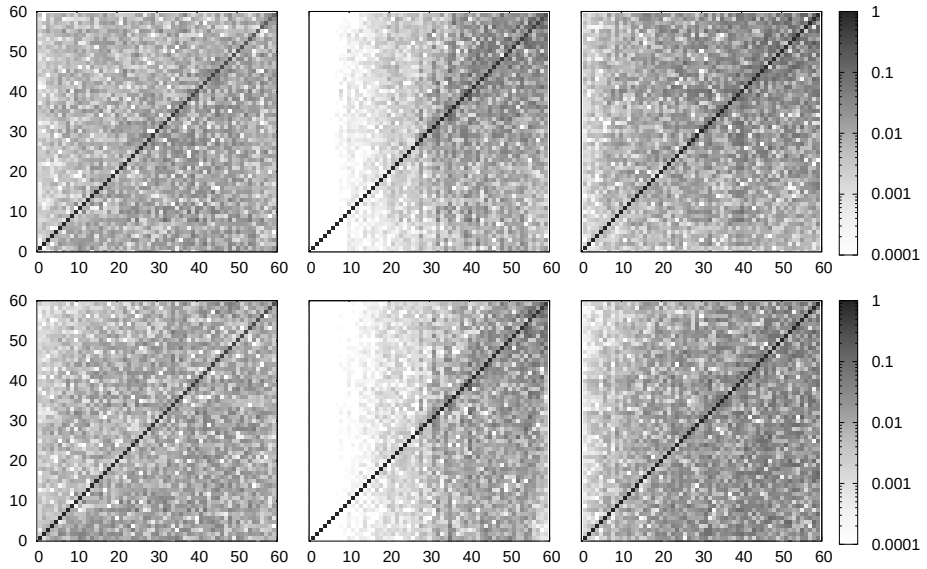

Figure 19: Dispersion tests on mesh2 with faces stencils and EC. Top: CDLF, bottom: Box. Columns, from left to right: C, M, R.

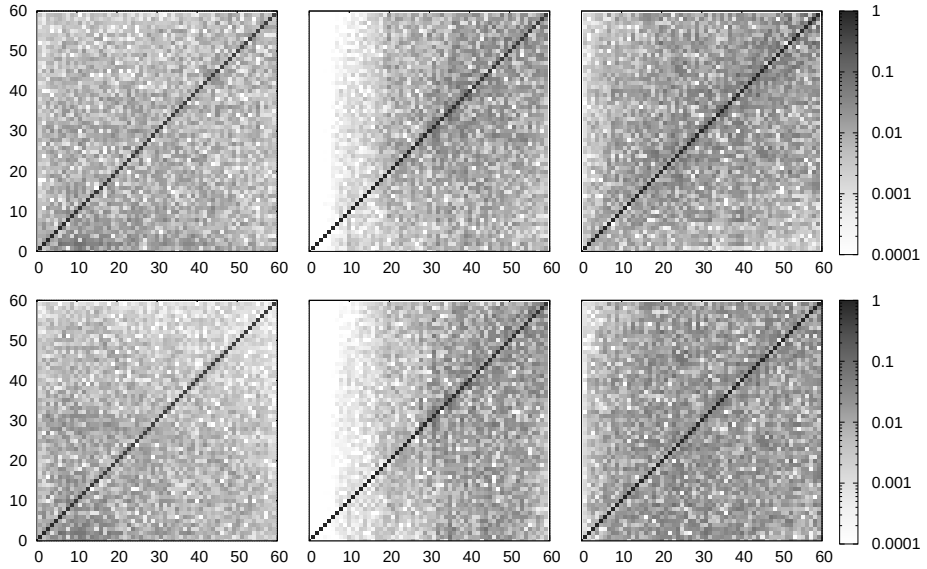

Figure 20: Dispersion tests on mesh2 with vertices stencils and EC. Top: CDLF, bottom: Box. Columns, from left to right: C, M, R.

distinguishable and the effect of the stencil is almost irrelevant regardless of the mesh.

Finally, in Figure 21, a dispersion comparison between EC and LED is shown. Dispersion is qualitatively equal but EC keeps, for all j, $(\hat{l}_i)_j/(\hat{l}_i)_i$ relatively lower than LED, so dispersion is lower. Such behavior has been observed with all meshes and filter drivers. It is attributed to the lower filter strength limit of EC.

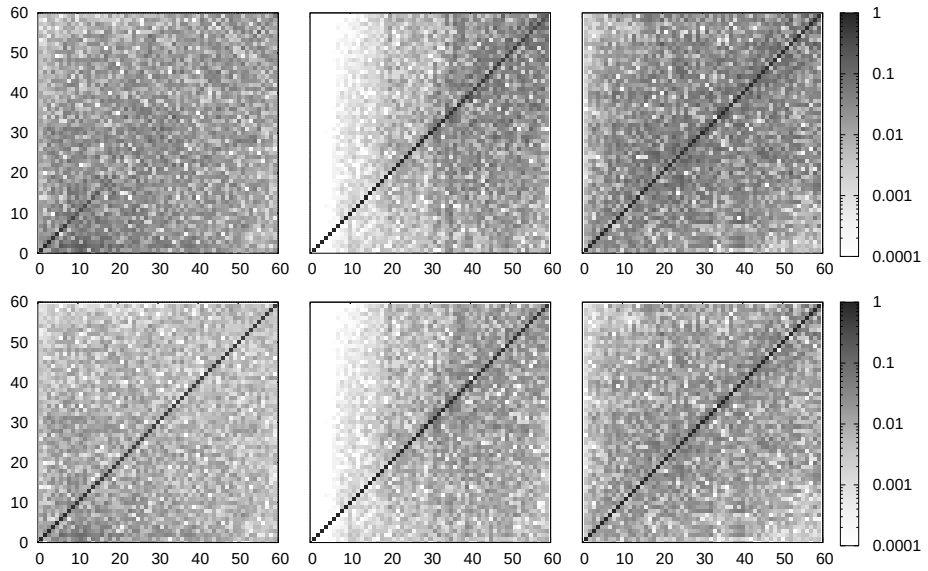

Figure 21: Projection tests on mesh2 with CLF with vertices stencils. Top: LED condition, bottom: EC condition. Columns, from left to right: C, M, R.

4.4. Tests on a singularity

Filtering of a singularity field has been carried out in order to compare EC to LED variations reduction constraints. This test consists on filtering a field evaluating 0 in all CV but one near the center of the mesh where it evaluates 1. Tests are performed on mesh1 and mesh2 with constant filter strength parameters. The value of the filter parameter is 2 for the reference Laplacian filter while for the other filters it has been adapted as detailed in Appendix C. The variations reduction limit on the filter strength parameter has been imposed with Inequality (31) on CLF, with Inequality (36) on CDLF and SDLF and as it is described in Appendix A for Box and Laplacian. Figures 22 and 23 show the filtered fields. With the LED constraint, the neighbors of the singularity become maxima after filtering while, as it has been predicted in Section 2.7, EC avoids it. After the results, EC filters seem more appropriate for cases with singularities or elements with very sharp gradients like the body forces of the Actuator Line Method (see, e.g. [27]) and the Immersed Boundary Methods (see, e.g. [16]). It also seems that vertex stencils are better fitted for these cases as they spread singularities on areas with rounder shapes, better approaching analytic filtering in continuous spaces.

Figure 22: Filtered singularity on mesh1, brighter gray shades are higher values. LED (top) vs. EC (bottom) restrictions. From left to right: Box, BoxV, Laplacian, LaplacianV, CLF, CLFV, CDLF, CDLFV, SDLF, SDLFV.

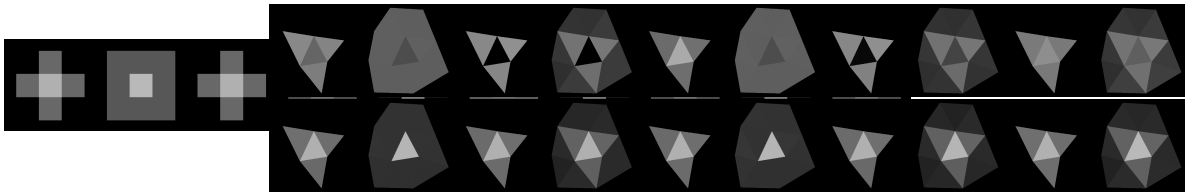

Figure 23: Filtered singularity on mesh2, brighter gray shades are higher values. LED (top) vs. EC (bottom) restrictions. From left to right: Box, BoxV, Laplacian, LaplacianV, CLF, CLFV, CDLF, CDLFV, SDLF, SDLFV.

4.5. Tests on a 2D isentropic vortex

Vortices are the simplest flow structure in cases without sources or sinks and one of the basic flow elements of inviscid potential flow approximations. We filter a 2D isentropic vortex to study the effect of the introduced filters on a typical configuration with physical relevance. The vortex velocity field is:

$$\mathbf{u} = u_a \exp\left(\frac{1-r^2}{2}\right)\left\{\begin{array}{c}\eta\\-\xi\end{array}\right\}. \tag{39}$$

with $\xi = (x - x_0)/b$, $\eta = (y - y_0)/b$ and $r^2 = \xi^2 + \eta^2$, b is a parameter determinative of the vortex size and u_a determines the vortex intensity. We use $u_a = 1$ and $b = 0.2/\sqrt{\log(2)}$ on the unitary square sided 2D meshes, where the vortex is centered.

The analytic filtered vortex field is, according to Equation (8):

$$\hat{\mathbf{u}}^* = u_a \exp\left(\frac{1-r^2}{2}\right)\left\{\begin{array}{c}\eta + \frac{\varepsilon^2}{24b^2}(-1-2\eta+\xi^2\eta+\eta^2)\\-\xi + \frac{\varepsilon^2}{24b^2}(-1+2\xi-\xi\eta^2+\xi^2)\end{array}\right\}. \tag{40}$$

We perform two different tests: the first aims to provide data for comparison of filters and the second aims to evaluate the accuracy of the filters on similar meshes with appreciably different numbers of cells, i.e. cell sizes. For both of them, we use the EC variations reduction condition for all computations and the constant input filter parameter $\epsilon = \sqrt{2}$.

In the first test, various relevant magnitudes are calculated from the filtered fields obtained with the filters introduced in former sections. These magnitudes are circulation, error with respect the analytical solution, total variations with

respect to the unfiltered field and average, maximum and minimum horizontal velocity. Circulation is computed as

$$\Gamma = \frac{\sum_o \Omega_o (uy - vx)_o}{\sum \Omega_o}, \tag{41}$$

TV as

$$TV = \frac{1}{2}\left(\frac{\sum_{\underline{op}} |\hat{u}_o - \hat{u}_p|}{\sum_{\underline{op}} |u_o - u_p|} + \frac{\sum_{\underline{op}} |\hat{v}_o - \hat{v}_p|}{\sum_{\underline{op}} |v_o - v_p|} \right), \tag{42}$$

and the error as

$$Err = \frac{1 + V_{in}/V_{bound}}{V_{in} + V_{bound}} \frac{\sum_{o \in in} ||\hat{\mathbf{u}}_o - \hat{\mathbf{u}^*}_o|| \Omega_o^{1/3}}{\sum \Omega_o}, \tag{43}$$

upon which some considerations follow.

Since the effective filtering effect is proportional to $(\epsilon\Delta)^2$ and so is $||\hat{\mathbf{u}^*}_o - \hat{\mathbf{u}}_o|| = ||(\hat{\mathbf{u}^*}_o - \mathbf{u}_o) - (\hat{\mathbf{u}}_o - \mathbf{u}_o)||$, we scale the volume averaged error dividing it by the square of local characteristic lengths, i.e., $\Omega_o^{2/3}$. Doing thus, the filtering strength dependence on the mesh is prevented from blurring the results. Furthermore, as at cells next to boundaries the filters are far from reproducing Laplacians, the total error would be dominated by the error on these cells if they were taken into account. Hence, only cells with no boundary faces are included in the sum of Equation (43). After this, the error gets blurred again by the difference of volumes of the meshes without boundary cells. We define V_{in} as the sum of the volumes of all cells without boundary faces and V_{bound} as the sum of the volumes of all cells with boundary faces to add an scaling factor that resolves the problem. After all these considerations, the error is only due to differences between filters spatial discretizations and analytic Laplacians. It is expected to increase with coarser meshes as the discrete representation of the vortex becomes less accurate.

Results of the first test on mesh1 are shown on Table 1. Laplacian, CLF, CDLF and SDLF are the same filter on this mesh. Filters with vertex stencils cause a more noticeable reduction of extrema of the horizontal velocity than those with face stencils. This was already observed and explained in tests on variations evolutions. It is also relevant that the error committed with respect to the analytic filter with vertex stencils is orders of magnitudes higher than the error committed with face stencils. This shows that the method developed in Section 3.3 to extend filters to vertex stencils does not accurately approximate the Laplacian operator. However, as stated before, we do not consider this a determinative criterion when designing filters. Comparing filters with face stencils, all excepting Box give the same results because the filter parameters were adjusted to do this. The discrepancies of the Box filter on all magnitudes but Err is because the different number of neighbors of boundary cells is not taken into account when calculating filter strength parameters. This was already observed in previous tests. We also remark that the Box filter does not reduce Γ and BoxV increases it. Finally, it is noticeable that non-conservative filters can change the average of the horizontal velocity on its order of magnitude.

Results with mesh2 are on Table 2. Vertices stencils produce larger errors than faces stencils but they are on the same order of magnitude. Actually, on this 2D test, they keep a ratio next to 10/3. This can be related to the ratio of the numbers of neighbor cells that each stencil involves. The conservation behavior is the expected. Again, non conservative filters change $\overline{U}$ on its order of magnitude. Circulation is not reduced by LaplacianV and it is significantly increased by Box, showing the difficulty of filtering on unstructured meshes.

Filter	Γ	Err	TV	$\overline{U}$	U_{max}	U_{min}
noFilter	0.215	2.67	1	-1.24e-10	0.977	-0.977
Analytic	0.211	0	0.955	-3.84e-11	0.936	-0.936
Laplacian	0.214	0.114	0.948	7.23e-11	0.938	-0.938
LaplacianV	0.213	2.67	0.89	5.79e-10	0.897	-0.897
Box	**0.215**	1.19	0.914	-3.44e-10	0.919	-0.919
BoxV	**0.217**	2.97	0.867	-1.18e-10	0.892	-0.892
CLF	0.214	0.114	0.948	-1.24e-10	0.938	-0.938
CLFV	0.212	2.97	0.887	-1.24e-10	0.892	-0.892
CDLF	0.214	0.114	0.948	-1.24e-10	0.938	-0.938
CDLFV	0.213	2.67	0.893	-1.24e-10	0.897	-0.897
SDLF	0.214	0.114	0.948	1.71e-10	0.938	-0.938
SDLFV	0.213	2.67	0.893	4.95e-10	0.897	-0.897

Table 1: Results of some relevant parameters after filtering vortex on mesh1.

Filter	Γ	Err	TV	$\overline{U}$	U_{max}	U_{min}
noFilter	0.219	2.61	1	-0.00644	0.999	-0.986
Analytic	0.211	0	0.926	-0.00191	0.936	-0.87
Laplacian	0.218	0.913	0.901	-0.00651	0.932	-0.891
LaplacianV	**0.219**	3.44	0.801	-0.00405	0.855	-0.777
Box	**0.223**	2.06	0.898	-0.015	0.921	-0.864
BoxV	0.216	5.42	0.789	-0.0141	0.835	-0.731
CLF	0.218	1.36	0.943	-0.00644	0.959	-0.933
CLFV	0.211	4.46	0.808	-0.00644	0.836	-0.784
CDLF	0.218	1.12	0.904	-0.00644	0.929	-0.899
CDLFV	0.214	3.78	0.838	-0.00644	0.837	-0.856
SDLF	0.218	0.897	0.905	-0.00582	0.936	-0.886
SDLFV	0.211	3.98	0.826	0.0092	0.837	-0.794

Table 2: Results of some relevant parameters after filtering vortex on mesh2.

There are no remarkable accuracy differences between the developed filters and the previously existing ones.

The objective of the second test is to compare the accuracy of the different filters on uniform and unstructured meshes with significantly different numbers of cells. To do it, two structured Cartesian meshes with 25 and 225 CV respectively and two unstructured meshes with 25 and 177 CV are additionally employed. Volumes thickness is set with the same criterion as it has been done with mesh1 and mesh2 so the characteristic length of mesh cell equals ${N_{cells}}^{-0.5}$.

The Error calculated with Equation (43) is plotted as a function of the number of cells of the meshes on Figure 24. With structured meshes, the error tends to zero as the number of cells increases when using faces stencils while it does not vary with a recognizable trend with vertex stencils. A clear trend is not observed for any stencil or filter on the unstructured meshes plot. The only clear conclusion from the vertex stencils plot is that vertex stencils produce larger errors than face stencils. Finally, we highlight that the dependence on meshes of the results obtained with filters developed in section 3 is not significantly different to that of the the corresponding Box or Laplacian filters.

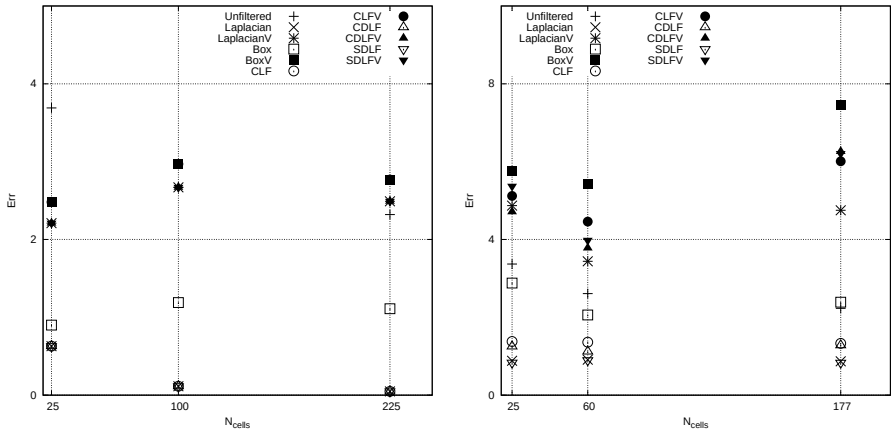

Figure 24: Error with respect to analytical filtering computed with equation (43) as a function of the number of cells. Left: Cartesian meshes. Right: Unstructured meshes. The average characteristic cell length is ${N_{cells}}^{-0.5}$

.

5. Conclusions and future work

The properties of the analytical convolution filter have been revised together with other analytical filter models used in CFD have been revised. The properties of the convolution filter that we have considered more characteristic of filtering have been adapted to discrete operators. Then, constraints enforcing them have been derived. Vreman [31] related normalization and conservation to the conservation of momentum and dissipation of kinetic energy in the context of LES. We have derived and successfully imposed these properties without need of relating filters to specific applications. It has been shown, by means of an example, that LED (positivity in [32]) is not sufficient to reproduce the diffusivity of the analytic models. Total Variation Diminishing of order 1 has been suggested as an objective diffusivity enforcing restriction but we could not theoretically impose it. We could not impose it TVD_2 for all input fields either. Diffusivity, however, has been approached with two different conditions: LED and EC. LED has been found to lead to the same condition as preventing the growth of the square of the Euclidean norm of the gradient for eigenvectors of the filter operator. EC mimics the second law of thermodynamics in heat transfer problems and is more restrictive than LED.

Three filters have been designed to satisfy one of the variations restrictions, normalization and conservation or symmetry. These filters have been implemented with faces-neighbors and vertex-neighbors stencils.Then, they have been tested alongside with a Laplacian and a Box filters.

Tests on the basic properties have been conducted using the eigenvectors of the graph Laplacian matrix of meshes as the tested fields because they are a good basis to represent oscillations scales. Results show TV_1 on most cases even when EC or LED (instead of TVD_1) is imposed. Still, low oscillated fields and filters active only on some cells result on relative TV_1 growths of 10^{-3} in the case of EC and 10^{-2} in the case of LED. Since the pathological settings (smooth fields and sharp variations of filtering intensity) are not usual in CFD, we consider the proposed variations restrictions surprisingly satisfactory. Tests also show that filters for which conservation is not imposed are not conservative. Dispersion tests show that LED and EC are also useful to bound the amount of dispersion that filtering produces between the modes of meshes and that lesser dispersion is obtained with EC because it is more constraining. In summary, tests results confirm that the developed filters are good candidates to be used in most of the CFD applications and that LED and EC conditions can restrain TV_1 growth in almost all relevant CFD cases.

The proposed and the previously existing filters have been also tested on singularity fields providing results that show the advantage of EC over LED in cases with very steep gradients. While LED allows dislocation of extrema, EC does not. Thereby, it is in better consonance with the properties of the introduced analytic filters.

Further tests on an isentropic vortex show that the introduced filters, compared to existing ones, do not increase local errors. However, it has been seen that the local inaccuracy with respect to the analytical explicit differential second order models in Sagaut and Grohens [23] of the studied filters increases with unstructured meshes and vertex stencils. We do not believe this is a major inconvenience as we consider that operators should be first approximated in their characterizing global properties and later provided with local accuracy. For example, the introduced CDLF with vertex stencils leads to high local errors with respect to the analytic model it's based on but it is conservative and normalized. These are properties of the analytic model that Least Squares approximations to Laplacians do not respect.

Tests on the isentropic vortex have also shown that the Box, BoxV and Laplacian filters can increase vortex circulation even when the EC constraint is imposed. This could cause a malfunction to LES models that use them, so our opinion is that further research on filters effect to this kind of simple relevant configurations should be performed.

The proposed restrictions are expected to be a good starting point for filter design. Then, specific applications require further conditions that should be compatible with those developed here. For example, commutation with differentiation is characteristic of convolution but not of all other analytical filter models and this is why we did not consider it a filter characterizing property. Meanwhile

conservation is equivalent to normalization in convolution and characterizing of most of the analytical models presented in this work, so we recommend to impose is not always imposed on discrete filters in the literature. To us, after the results on the isentropic vortex where it is shown that non-conservative filters can increase circulation, an effort should be made to clarify if relaxing conservation allows for physically consistent filters. Low dispersion and TVD_1 remain objective properties as we could not explicitly impose them. However, smoothing of any input field, which is the most basic consequence of filtering, has been practically attained for compact supported explicit filters with the EC condition.

We emphasize the capabilities of the proposed testing techniques introduced in this document to better separate and identify the performance of filters on each field mode for all types of meshes. We consider that research on filters should try to find better tests to isolate, as much as possible, filter behavior from any other operation. In this sense, substituting the eigenvectors of the graph Laplacian matrix by those of some volume-weighted symmetric semidefinite matrices with physical relevance could improve the oscillations measurements performed here. This would take into account spatial variables while avoiding the inconveniences of the differential operators on unstructured meshes.

Most of the paper is focused on FV and finite discrete space, but all the theories and properties studied can be easily extended to general Hilbert spaces or other discretizations.

Future work will focus on the use of the proposed filters in actual CFD simulations.

Acknowledgments

Fred Wubs and Maurits Silvis from the University of Groningen are kindly acknowledged for their advices. This work has been financially supported by the Spanish Ministerio de Economía y Competitividad through the grant BES-2010-032414, the research program ENE-2012-36910 and the Ramón y Cajal postdoctoral contract RYC-2012-11996.

Bibliography

[1] Christophe Bogey, Nicolas de Cacqueray, and Christophe Bailly. A shock-capturing methodology based on adaptative spatial filtering for high-order non-linear computations. *Journal of Computational Physics*, 228(5):1447–1465, 2009.

[2] M. Calaf, C. Meneveau, and J. Meyers. Large eddy simulation study of fully developed wind-turbine array boundary layers. *Physics of Fluids*, 22(2010):015110, 2010.

[3] Bjorn Engquist, Per Lotstedt, and Bjorn Sjogreen. Nonlinear filters for efficient shock computation. 52(186):509–537, 1989.

[4] Mark Galassi, Jim Davies, Brian Gough, Gerard Jungman, Patrick Alken, and Rhys Ulerich. GNU Scientific Library, 2015.

[5] M. Germano. Differential filters for the large eddy numerical simulation of turbulent flows. *Physics of Fluids*, 29:1755, 1986.

[6] M. Germano. Turbulence - The filtering approach. *Journal of Fluid Mechanics*, 238, 1992.

[7] Massimo Germano, Ugo Piomelli, Parviz Moin, and William H. Cabot. A dynamic subgrid-scale eddy viscosity model. 1760(May 2013), 1990.

[8] S. Ghosal and P. Moin. The Basic Equations for the Large Eddy Simulation of Turbulent Flows in Complex Geometry, 1995.

[9] Ami Harten. High Resolution Schemes for Hyperbolic Conservation Laws. *Journal of Computational Physics*, 135:260–278, 1983.

[10] Andreas Haselbacher and Oleg V. Vasilyev. Commutative discrete filtering on unstructured grids based on least-squares techniques. *Journal of Computational Physics*, 187(1):197–211, 2003.

[11] Thomas J.R. R Hughes, Luca Mazzei, and Kenneth E. Jansen. Large Eddy Simulation and the variational multiscale method. *Computing and Visualization in Science*, 3:47–59, 2000.

[12] O. Lehmkuhl, I. Rodríguez, R. Borrell, and A. Oliva. Low-frequency unsteadiness in the vortex formation region of a circular cylinder. *Physics of Fluids*, 25(8):85109, 2013.

[13] B. P. Leonard. A stable and accurate convective modelling procedure based on quadratic upstream interpolation. *Computer Methods in Applied Mechanics and Engineering*, 19(1):59–98, 1979.

[14] T. S. Lund. The Use of Explicit Filters in Large Eddy Simulation. *Computers and Mathematics with Applications*, 46:603–616, 2003.

[15] Alison L Marsden, Oleg V Vasilyev, and Parviz Moin. Construction of Commutative Filters for LES on Unstructured Meshes. *Journal of Computational Physics*, 175:584–603, 2002.

[16] Rajat Mittal and Gianluca Iaccarino. Immersed Boundary Methods. *Annual Review of Fluid Mechanics*, 37:239–261, 2005.

[17] J. S. Mullen and P. F. Fischer. Filtering techniques for complex geometry fluid flows. *Communications in Numerical Methods in Engineering*, 15:9–18, 1999.

[18] Noma Park, Sungwon Lee, Jungil Lee, and Haecheon Choi. A dynamic subgrid-scale eddy viscosity model with a global model coefficient A dynamic subgrid-scale eddy viscosity model with a global model coefficient. 125109(18), 2006.

[19] J. Blair Perot. Discrete Conservation Properties of Unstructured Mesh Schemes. *Annual Review of Fluid Mechanics*, 43(1):299–318, 2011.

[20] RS S Rogallo and Parviz Moin. Numerical simulation of turbulent flows. *Annual Review of Fluid Mechanics*, 16:99–137, 1984.

[21] W Rozema, J.C. C Kok, R.W.C.P. Verstappen, and A.E.P. E P Veldman. A symmetry-preserving discretisation and regularisation model for compressible flow with application to turbulent channel flow. *Journal of Turbulence*, 15(March 2015):386–410, 2014.

[22] Leonid I. Rudin, Stanley Osher, and Emad Fatemi. Nonlinear total variation based noise removal algorithms. *Physica D: Nonlinear Phenomena*, 60:259–268, 1992.

[23] P. Sagaut and R. Grohens. Discrete filters for large eddy simulation. *International Journal for Numerical Methods in Fluids*, 31(October 1997):1195–1220, 1999.

[24] Pierre Sagaut. *Large eddy simulation for incompressible flows: an introduction*. 2006.

[25] F. X. Trias, a. Gorobets, a. Oliva, and C. D. Pérez-Segarra. DNS and regularization modeling of a turbulent differentially heated cavity of aspect ratio 5. *International Journal of Heat and Mass Transfer*, 57(1):171–182, 2013.

[26] F. X. Trias and R. W C P Verstappen. On the construction of discrete filters for symmetry-preserving regularization models. *Computers and Fluids*, 40(1):139–148, 2011.

[27] Niels Troldborg, Jens N Sørensen, and Robert Mikkelsen. Actuator Line Simulation of Wake of Wind Turbine Operating in Turbulent Inflow. *Journal of Physics: Conference Series*, 75:12063, 2007.

[28] Oleg V. Vasilyev, Thomas S. Lund, and Parviz Moin. A general class of commutative filters for LES in complex geometries. *Journal of Computational Physics*, 146:82–104, 1998.

[29] R. W. C. P. Verstappen and A. E. P. Veldman. Symmetry-preserving discretization of turbulent flow. *Journal of Computational Physics*, 187:343–368, 2003.

[30] Roel Verstappen. On restraining the production of small scales of motion in a turbulent channel flow. *Computers & Fluids*, 37:887–897, 2008.

[31] A. W. Vreman. The adjoint filter operator in large-eddy simulation of turbulent flow. *Physics of Fluids*, 16(6):2012–2022, 2004.

[32] Bert Vreman, Bernard Geurts, and Hans Kuerten. Realizability conditions for the turbulent stress tensor in large-eddy simulation. *Journal of Fluid Mechanics*, 278:351, 1994.

[33] Bert Vreman, Bernard Geurts, and Hans Kuerten. Large-eddy simulation of the turbulent mixing layer. *Journal of Fluid Mechanics*, 339:357–390, 1997.

[34] H. C. Yee. A Class of High-Resolution Explicit and Implicit Shock-Capturing Methods. (February), 1994.

[35] Donghyun You and Parviz Moin. A dynamic global-coefficient subgrid-scale eddy-viscosity model for large-eddy simulation in complex geometries. *Physics of Fluids*, 19(6):1–8, 2007.

Appendix A. Tested filters

Adaptative filters are controlled at each o cell by a filter ratio ϵ_o parameter or a characteristic cut-off $\epsilon_o\Delta_o$ length. To ensure the accomplishment of conditions of Section 2, limitations on ϵ_o are imposed. Descriptions of filters used in 4 and the bounds imposed on their filter ratios are included in this appendix.

Appendix A.1. The Laplacian filter

The Laplacian filter used in this work is an adaptation to any mesh of the differential filter that approximates convolution filters in [23]. It reads:

$$\hat{\phi}_o = \phi_o + \frac{(\epsilon_o \Omega_o^{1/3})^2}{24\Omega_o} \sum_{p \in N_o} (\phi_p - \phi_o) \frac{A_{\underline{op}}}{\boldsymbol{n}_{\underline{\boldsymbol{op}}} \cdot \boldsymbol{r}_{\underline{\boldsymbol{op}}}} \tag{A.1}$$

Where $A_{\underline{op}}$ is the area of the interface between the o and p control volumes, $\boldsymbol{n}_{\underline{\boldsymbol{op}}}$ is the unitary vector normal to the interface oriented from o to p and $\boldsymbol{r}_{\underline{\boldsymbol{op}}}$ is the vector from the cell center of o to the cell center of p. Here, the characteristic $\Delta_o = \Omega_o^{1/3}$, and Ω_o is the volume of the o cell. LED or EC criteria can be imposed with:

$$\epsilon_o^2 \leq \frac{24\Omega_o^{1/3}}{\sigma \sum_{p \in N_o} \frac{A_{\underline{op}}}{\boldsymbol{n}_{\underline{\boldsymbol{op}}} \cdot \boldsymbol{r}_{\underline{\boldsymbol{op}}}}} \tag{A.2}$$

Where $\sigma = 1$ to impose LED and $\sigma = 2$ to impose EC. Tests in Section 4 have been conducted using this limitations.

Appendix A.2. The Box filter

The Box filter is computed as an averaging of the values of a neighborhood of a CV. It is the adaptative version of the filter in [31].

$$\hat{\phi}_o = \frac{1}{\epsilon_o} \left(\phi_o + \frac{(\epsilon_o - 1)}{\sum_{p \in N_o} \Omega_p} \sum_{p \in N_o} \phi_p \Omega_p \right) \tag{A.3}$$

LED is imposed with $1 \leq \epsilon_o$ and EC with $1 \leq 2$. This restrictions have been applied on tests described in Section 4.

Appendix B. Filter TVD analysis on the infinitesimal filter limit

Conditions (19) and (21) in Section 2.7 are equivalent. For a general filter, the elements of K of equation (21) read:

$$k_{o\,o} = \overline{\overline{N_o}} - f_{o\,o}^2 \overline{\overline{N_o}} - \sum_{p \in N_o} f_{p\,o} \left(\overline{\overline{N_p}} f_{p\,o} - 2 f_{o\,o} - \sum_{q \in N_o \cap N_p} f_{q\,o} \right) \tag{B.1}$$

$$k_{o\,p} \overset{*}{=} -1 - f_{o\,p} \left(\overline{\overline{N_o}} f_{o\,o} - \sum_{q \in N_o} f_{q\,o} \right) - f_{p\,p} \left(\overline{\overline{N_p}} f_{p\,o} - f_{o\,o} - \sum_{q \in N_o \cap N_p} f_{q\,o} \right) - ... \\ ... - \sum_{q \in No \cap N_p} f_{q\,p} \left(\overline{\overline{N_q}} f_{q\,o} - f_{o\,o} - \sum_{r \in N_o \cap N_q} f_{r\,o} \right) + \sum_{\substack{q \in N_p \\ q \notin N_o}} f_{q\,p} \sum_{r \in N_o \cap N_q} f_{r\,o} \tag{B.2}$$

$$k_{o\,q} \overset{**}{=} -1 + \sum_{p \in N_o \cap N_q} \left[f_{p\,o} f_{q\,q} - f_{p\,q} \left(N_p f_{p\,o} - f_{o\,o} - \sum_{r \in N_o \cap N_p} f_{r\,o} \right) \right] \tag{B.3}$$

Equality (B.2) stands for $p \in N_o$ while equality (B.3) stands for $q \in N_p$ with $p \in N_o$ and $q \notin N_o$. Now, we perform an analysis for normalized filter matrices F with $f_{o\,p} = \varepsilon f_{o\,p}^*$ and $f_{o\,o} = 1 - \varepsilon \sum_{p \in N_o} f_{o\,p}^*$. Parameter $\varepsilon \ll 1$ is positive and $f_{o\,p}^* \sim 1 \quad \forall o \neq p$. We write $S_o = \sum_{q \in N_o} f_{o\,q}^*$, $R_o = \sum_{q \in N_o} f_{q\,o}^*$ and $T_{o\,p} = \sum_{q \in N_o \cap N_p} (f_{q\,o}^* + f_{q\,p}^*)$. With them, we get:

$$\lim_{\varepsilon \to 0^+} k_{o\,o} = \lim_{\varepsilon \to 0^+} 2\varepsilon \left(\overline{\overline{N_o}} S_o + R_o \right) + \mathcal{O}(\varepsilon^2) \simeq 0^+ \tag{B.4}$$

$$\lim_{\varepsilon \to 0^+} k_{o\,p} \overset{*}{=} \lim_{\varepsilon \to 0^+} -\varepsilon \left(\overline{\overline{N_o}} f_{o\,p}^* + S_o + \overline{\overline{N_p}} f_{p\,o}^* + S_p - T_{o\,p} \right) + \mathcal{O}(\varepsilon^2) \simeq 0^- \tag{B.5}$$

$$\lim_{\varepsilon \to 0^+} k_{o\,q} \overset{**}{=} \lim_{\varepsilon \to 0^+} \varepsilon \sum_{p \in N_o \cap N_q} \left(f_{p\,q}^* + f_{p\,o} \right) + \mathcal{O}(\varepsilon^2) \simeq 0^+ \tag{B.6}$$

Now, for K to be $\succeq 0$, it should be Diagonal Dominant, so

$$\sigma_o = \lim_{\varepsilon \to 0^+} k_{o\,o} - \sum_{p \neq o} |k_{o\,p}| \simeq 2\varepsilon \left(\overline{\overline{N_o}} S_o + R_o \right) - ... \\ - \varepsilon \sum_{p \in N_o} \left(\overline{\overline{N_o}} f_{o\,p}^* + S_o + \overline{\overline{N_p}} f_{p\,o}^* + S_p - T_{o\,p} \right) + ... \\ ... + \varepsilon \sum_{\substack{q \in N_p \\ q \notin N_o \\ p \in N_o}} \sum_{p \in N_o \cap N_q} \left(f_{p\,q}^* + f_{p\,o}^* \right) \tag{B.7}$$

should be greater or equal to zero for all control volumes. We have studied various common situations on uniform 1D, 2D and 3D meshes. It has been found that only 1D filtering with only one neighbor leads to TVD filters for all input fields fields. Hence, K is not always diagonally dominant and we can not proof its positive definiteness. In conclusion, filters are not necessarily TVD at the infinitesimal limit. We remark that this result has been obtained with $||\mathsf{G}(\boldsymbol{\phi})||_2$ instead of $||\mathsf{G}(\boldsymbol{\phi})||_1$, which is the common TVD norm in the compressible flow literature.

Appendix C. Equivalences between filter strength parameters

The relationships between the filter widths, filter strength and filter ratios that, for constant meshes and filters, make the weights of neighbor cells equal are:

$$\varepsilon_B = \left(1 - \frac{\varepsilon_L^2 \overline{\overline{N}}}{24}\right)^{-1} \tag{C.1}$$

$$\varepsilon_{CLF} = \frac{\varepsilon_L^2}{24} \tag{C.2}$$

Where ε_B is the filter ratio of the Box filter, ε_{CLF} is the filter strength of the CLF filter, ε_L is the filter width of the Laplacian filters and $\overline{\overline{N}}$ is the average number of neighbors of the stencil. These relations apply for every cell of a constant mesh.

However, f_{oo} and f_{op} elements of the Box filters can not be equal to those of differential filters and the same time at cells near boundaries or cells with a number of neighbors in the stencil different to $\overline{\overline{N}}$. In any case, in order to compare filters with parameters "as equivalent as possible", we use relation (C.1).